AD-A122 477 BERING STRAIT SEA ICE AND THE FAIRWAY ROCK ICEFOOT(U) 1/1
COLD REGIONS RESEARCH AND ENGINEERING LAB HANOVER NH
A KOVACS ET AL. OCT 82 CRREL-82-31

UNCLASSIFIED F/G 8/12 NL

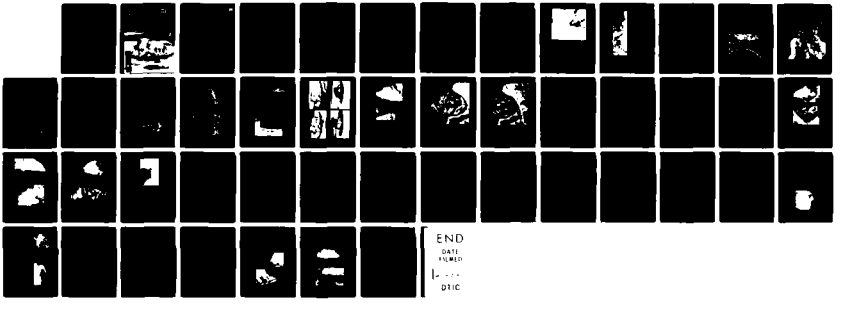

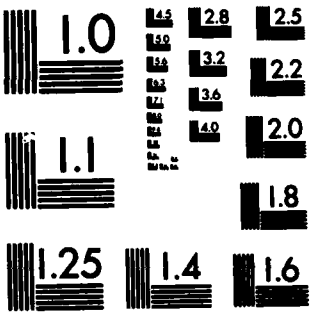

CRREL REPORT 82-31

US Army Corps of Engineers
Cold Regions Research & Engineering Laboratory

Bering Strait sea ice and the Fairway Rock icefoot

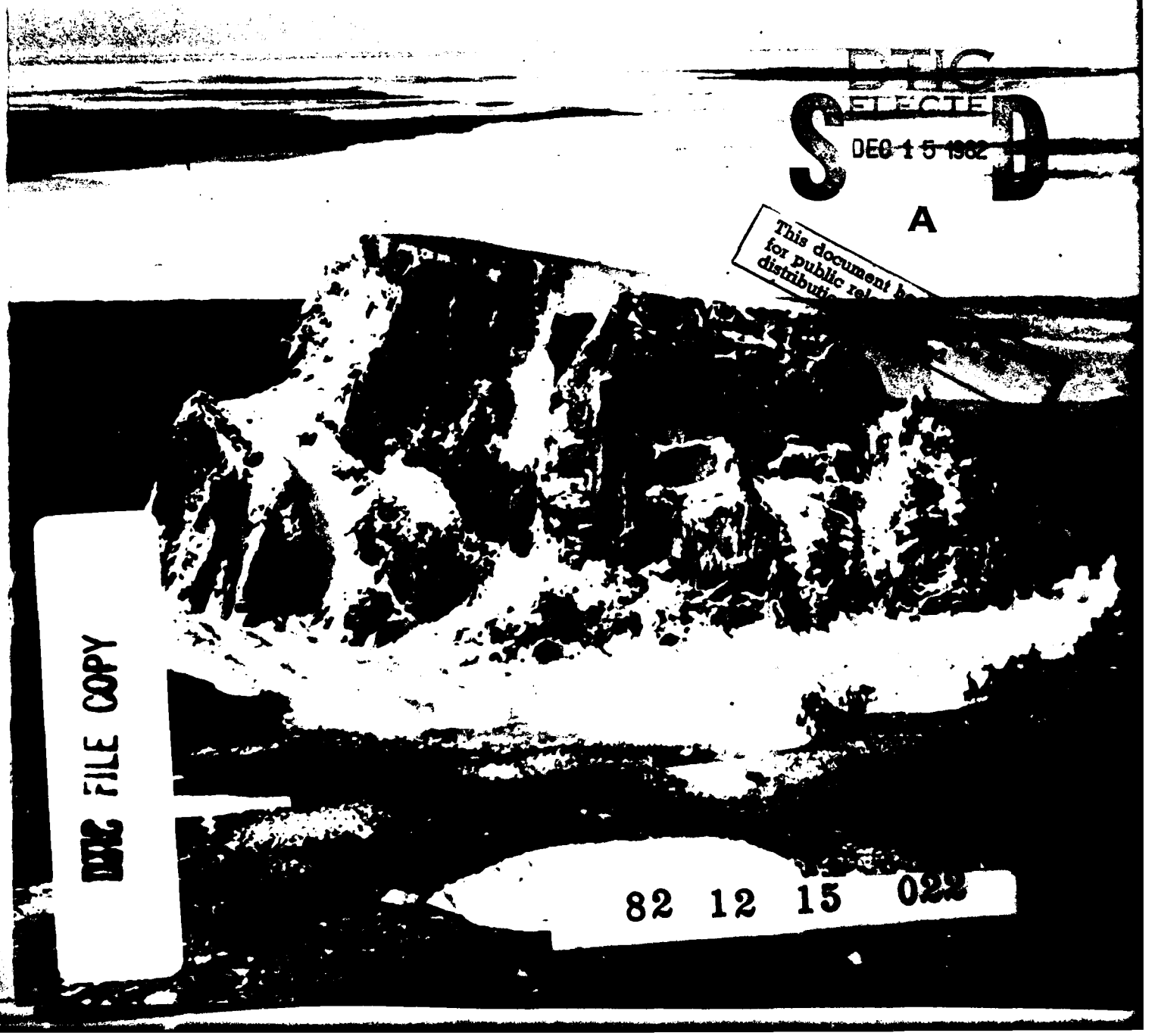

CRREL Report 82-31

October 1982

Bering Strait sea ice and the Fairway Rock icefoot

A. Kovacs, D.S. Sodhi and G.F.N. Cox

Unclassified

SECURITY CLASSIFICATION OF THIS PAGE (When Data Entered)

REPORT DOCUMENTATION PAGE		READ INSTRUCTIONS BEFORE COMPLETING FORM
1. REPORT NUMBER CRREL Report 82-31	2. GOVT ACCESSION NO. AD-A122 477	3. RECIPIENT'S CATALOG NUMBER
4. TITLE (and Subtitle) BERING STRAIT SEA ICE AND THE FAIRWAY ROCK ICEFOOT		5. TYPE OF REPORT & PERIOD COVERED 6. PERFORMING ORG. REPORT NUMBER
7. AUTHOR(s) A. Kovacs, D.S. Sodhi and G.F.N. Cox		8. CONTRACT OR GRANT NUMBER(s)
9. PERFORMING ORGANIZATION NAME AND ADDRESS U.S. Army Cold Regions Research and Engineering Laboratory Hanover, New Hampshire 03755		10. PROGRAM ELEMENT, PROJECT, TASK AREA & WORK UNIT NUMBERS
11. CONTROLLING OFFICE NAME AND ADDRESS U.S. Army Cold Regions Research and Engineering Laboratory Hanvoer, New Hampshire 03755		12. REPORT DATE October 1982 13. NUMBER OF PAGES 44
14. MONITORING AGENCY NAME & ADDRESS(if different from Controlling Office)		15. SECURITY CLASS. (of this report) Unclassified 15a. DECLASSIFICATION/DOWNGRADING SCHEDULE

16. DISTRIBUTION STATEMENT (of this Report)

Approved for public release; distribution unlimited.

17. DISTRIBUTION STATEMENT (of the abstract entered in Block 20, if different from Report)

18. SUPPLEMENTARY NOTES

Funded by
Gulf Canada Resources Inc.
Calgary, Alberta, Canada

Bureau of Land Management/
National Oceanic and Atmospheric
Administration
Washington, D.C.

19. KEY WORDS (Continue on reverse side if necessary and identify by block number)

Ice
Sea ice
Ice forces

20. ABSTRACT (Continue on reverse side if necessary and identify by block number)

Information on sea ice conditions in the Bering Strait and the icefoot formation around Fairway Rock, located in the strait, is presented. Cross-sectional profiles of Fairway Rock and the relief of the icefoot are given along with theoretical analyses of the possible forces active during icefoot formation. It is shown that the ice cover most likely fails in flexure as opposed to crushing or buckling, as the former requires less force. Field observations reveal that the Fairway Rock icefoot is massive, with ridges up to 15 m high, a seaward face only 20° from vertical, and interior ridge slopes averaging 33°. The icefoot is believed to be grounded and its width ranges from less than 10 to over 100 m.

DD FORM 1 JAN 73 1473 EDITION OF 1 NOV 65 IS OBSOLETE

Unclassified

SECURITY CLASSIFICATION OF THIS PAGE (When Data Entered)

PREFACE

This report was prepared by Austin Kovacs, Research Civil Engineer, Applied Research Branch, Experimental Engineering Division; Dr. Devinder S. Sodhi, Research Hydraulic Engineer, Ice Engineering Branch, EED; and Dr. Gordon F.N. Cox, Geophysicist, Snow and Ice Branch, Research Division of the U.S. Army Cold Regions Research and Engineering Laboratory.

Support for the study was provided by Gulf Canada Resources Incorporated, Calgary, Alberta, Canada, and by the Bureau of Land Management through an interagency agreement with the National Oceanic and Atmospheric Administration as part of the Alaska Outer Continental Shelf Environmental Assessment Program. The authors thank Douglas C. (Skip) Echert of Oceanographic Services Incorporated, who assisted with the aerial reconnaissance.

CONTENTS

ILLUSTRATIONS

TABLES

BERING STRAIT SEA ICE AND THE FAIRWAY ROCK ICEFOOT

A. Kovacs, D.S. Sodhi and G.F.N. Cox

INTRODUCTION

In the design of offshore structures to be placed in arctic waters, major consideration is being given to determining the loads developed during ice movement and failure against a structure. This could result in the creation of an ice rubble field which could increase the effective width of the structure and the forces transmitted to it. The phenomena of ice pile-up and over-ride are also major design considerations.

A variety of analytical and model studies have been made to investigate ice forces on offshore structures, but they are inconclusive, as their results have not been verified by field measurements. This paper presents the results of an investigation of the general configuration of ice rubble around Fairway Rock, Alaska. The purpose of the investigation was to acquire data on the morphology of the sea ice rubble surrounding the rock that would be applicable to offshore structures in general and to those placed in deep water in particular. Estimates of the relative force levels required to form the observed rubble are given. The surface relief across a number of sea ice rubble fields formed in the shear zone along the west side of Prince of Wales Shoal is described for the purpose of documenting the size of ice features which may impact offshore structures placed in the northern Bering Sea.

BERING STRAIT

The Bering Strait is 85 km wide and has an irregular bottom, with a depth of about 52 m near the western side and about 60 m near the eastern side. The bottom relief is probably the result of scouring by strong currents, ice gouging, and ancient river scouring (Selkregg 1976). On the western side of the strait is the formidably steep and rugged mountain topography of Cape Dezhneva and on the eastern side is the bold mountain landscape of Cape Prince of Wales. Winds in the strait tend to be funneled and accelerated in northerly or southerly directions by these headlands.

Within the Bering Strait are three islands (Fig. 1): Little and Big Diomede Islands and Fairway Rock. Fairway Rock, situated about 24 km west-southwest of Cape Prince of Wales, Alaska, is a 350-m-diameter igneous rock that rises almost vertically out of 50-m-deep water (G. Bloom, pers. comm.) to a height of about 165 m. Its top slopes gradually from the northwest to the southeast and is covered with a thin growth of hardy tundra grasses, lichens and mosses. At sea level, the island exhibits surfaces of near-vertical rock and steep talus slopes composed of large boulders. From the tidal zone to a depth of about 5 m ice abrasion inhibits marine growth (Fig. 2). Below this depth abundant flora and fauna exist (Shumway et al. 1964). In winter a very high pile of ice rubble surrounds the island. The lateral extent of this icefoot is limited by the abrupt drop-off of the island into deep water and by the erosional forces of drift ice, which pluck, cleave and grind away the ridged ice. Oceanographic instrument cables extending downward along the submarine boulder surface of the island have been extensively damaged to a depth in excess of 30 m by ice impact and abrasion (Bloom and McDougal 1967).

Fast ice extends offshore about 1 km at Cape

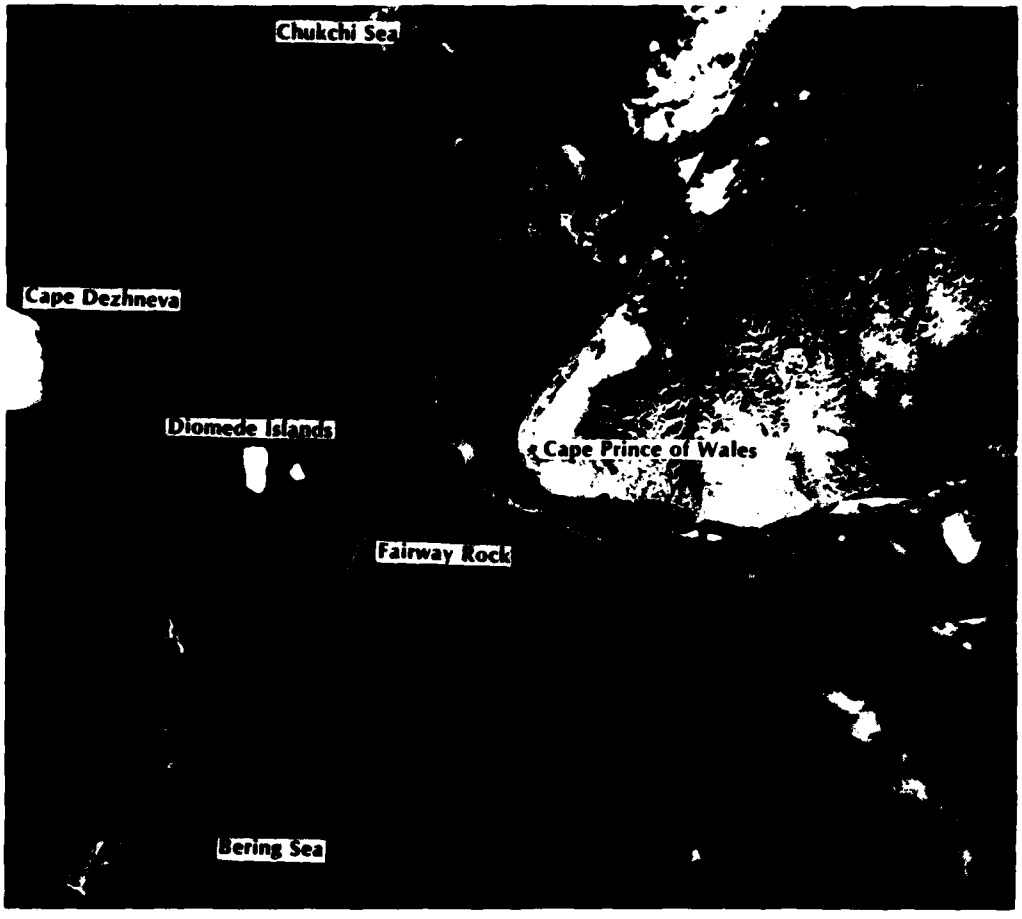

Figure 1. Landsat view of the Bering Strait on 22 June 1973.

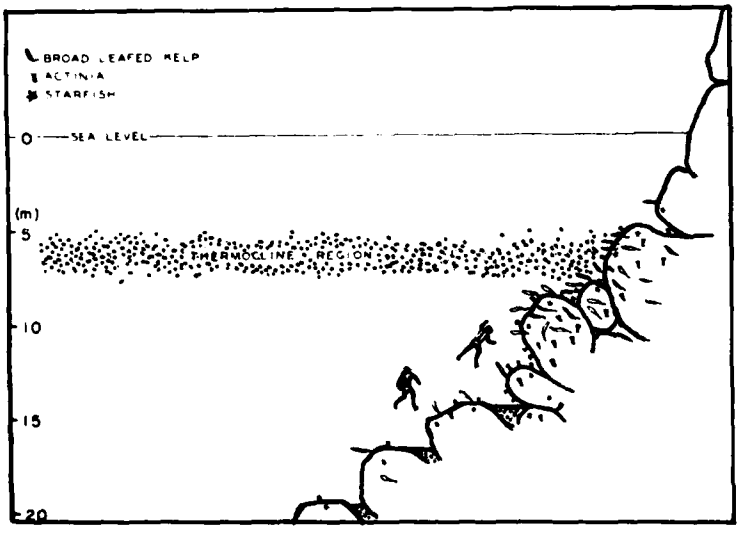

Figure 2. Representative underwater environment to a depth of 20 m at the south side of Fairway Rock (after Shumway et al. 1964).

Figure 3. Side-looking airborne radar image of 20 February 1980 showing Cape Prince of Wales and the sea ice in the shear zone north of the Bering Strait.

Prince of Wales and increases in width to the north. Its maximum thickness is about 1.4 m. All ice seaward of this shore-fast ice is in nearly constant motion. Along the western edge of the fast ice, extending in a general north-northeast direction, very long shear ridge-rubble fields form as a result of pack ice pressing in against the stable ice (Stringer 1978). These linear ice formations are easily visible in Figure 3. Many of the shear ridge fields have been estimated to be over 7 m high (Kovacs 1972). On Prince of Wales Shoal, which extends some 60 km in a northward direction from the eastern tip of Cape Prince of Wales, large, 14-m-high, isolated, grounded ice formations have also been observed (Kovacs 1972).

Oceanographic cables laid offshore at Cape Prince of Wales have been consistently cut or damaged by drift ice, usually during early freeze-up when pressure ridges develop along the fast ice edge or during spring breakup when grounded ice is pushed across the sea floor. Time domain reflectometry measurements on the broken cables have revealed that they are consistently damaged, beginning at about the 10-m depth and extending outward to about the 25-m depth. Sounding surveys have shown that ice gouging of the sea floor can be expected to a depth of 4 m, and that ice gouging extends out to about the 25-m water depth (Bloom and McDougal 1967).

Strong currents are characteristic of the Bering Strait flow regime. These currents consist of a semipermanent northward flow on the order of 0.8 ± 0.2 Sverdrup (Sv) (Coachman and Aagaard 1979). A downward sea surface slope of about 2.6×10^{-6} to the north is the primary mechanism responsible for this flow through the strait (Coachman and Aagaard 1966). However, wind and regional atmospheric pressure can cause significant spatial and especially temporal variation (on a time scale of days) in this flow, and major southerly flow can occur for short periods of time. If it were not for the strong southerly transport events, the annual northern transport would be higher by a factor of about 5. For example, between September 1976 and March 1977 there were 20 flow reversals, each lasting 6 to 12 days, for a total of 61 days. The transport-time record for this period (Fig. 4) shows that the largest transport through the strait occurred on 27 October. It was in a southerly (–) direction and had a volume of approximately 5.05 Sv, which for the Bering Strait is equivalent to a mean flow velocity of 4.4 km/hr (Coachman, pers. comm.). The largest northward transport of 3.15 Sv occurred on 7 January; mean flow velocity was 3.0 km/hr. The high flow veloci-

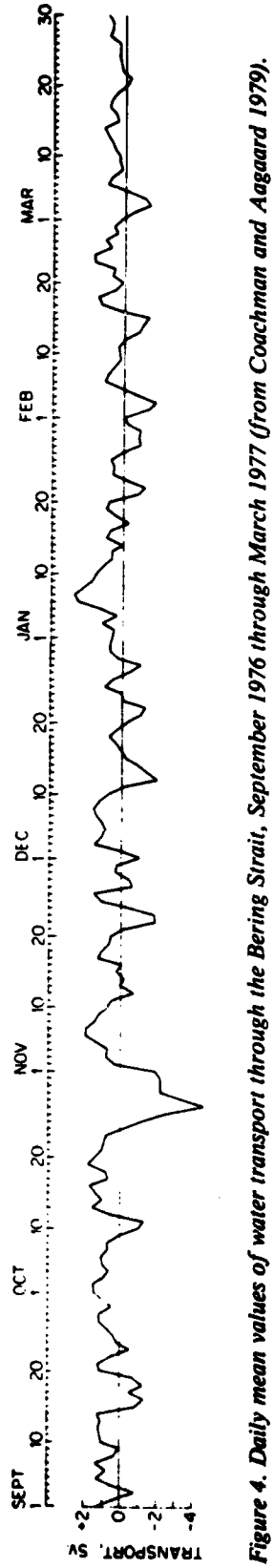

Figure 4. Daily mean values of water transport through the Bering Strait, September 1976 through March 1977 (from Coachman and Aagaard 1979).

ties which occur during these events may be the reason why More (1964) observed the sea floor to be essentially devoid of sediment for approximately 45 km northward of Little Diomede Island.

Coachman and Aagaard (1979) show that transport through the Bering Strait is well correlated with regional east-west atmospheric pressure differences (see Fig. 5): "When pressure on the east side (Nome, Kotzebue) is greater than on the west side (Provideniya Bukhts, Cape Serdtse-Kamen), the regional air flow is towards the north, as are the water transports, and vice versa. Southerly transport through the strait has a marked episodic character, and these events are caused by particular large scale atmospheric conditions. When a strong E-W pressure gradient lies over the strait and extends in a north-south direction from the Chukchi Sea to the central Bering Sea, entirely crossing the northern Bering Shelf, extensive northerly winds move water southward off the shelf. This produces a sea-level slope down to the south which, together with the northerly winds, drives southward transport. The atmospheric pressure pattern causing this condition is always a strong low located a considerable distance southeast of the strait (e.g. over Kodiak) together with the Siberian high, being centered some distance west of the strait."

Movement of ice southward through the Bering Strait is therefore driven by northerly winds and southerly current flow. The resulting coupling of the wind and current produces drag forces on the ice which exceed its arching strength. Thus the arched or jammed-up ice bridging the strait fails, and moves rapidly southward (Fig. 6 and 7). Two such events were studied by Ahlnäs and Wendler (1979). One event in January 1977 resulted in a mean estimated ice velocity through the strait of 4.1 km/hr. A second in March 1978 resulted in a mean ice velocity of 2.8 km/hr. These speeds are much higher than the typical speed of ice floes in the Bering Sea that have been tracked by satellite imagery. The latter always move at less than 1.1 km/hr and generally at less than 0.7 km/hr (Muench and Ahlnäs 1976).

Under strong driving forces acting over a prolonged period of time, sea ice in a belt 100 or more km wide, extending from the strait northward along the east side of the Chukchi Sea to Pt. Barrow and beyond, gradually moves southward (Fig. 8). In some years this movement brings multi-year ice floes into the northern Bering Sea. St. Lawrence Island natives interviewed at Gambell in April 1981 report seeing multi-year ice floes on occasion. During our reconnaissance flights we have

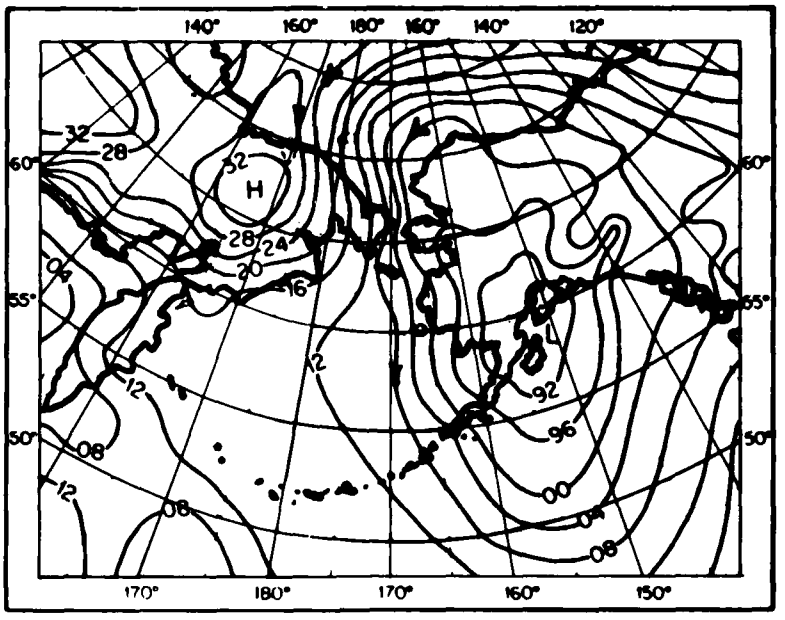

Figure 5. Atmospheric pressure pattern over Siberia and Alaska on 22 November 1976 (from Coachman and Aagaard 1979).

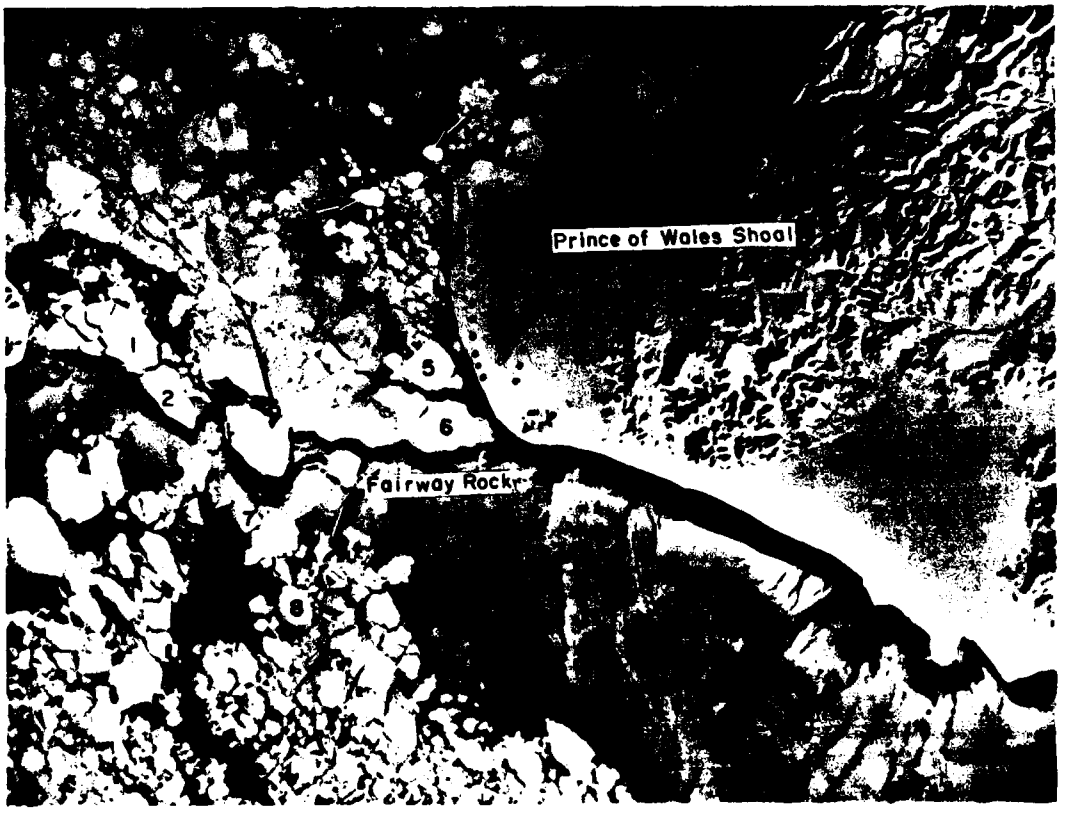

Figure 6. Floe conditions in Bering Strait on 6 March 197 at beginning of major rapid southern ice drift.

Figure 7. Ice conditions in Bering Strait on 7 March 1973. Note the position of the numbered ice floes in relation to their locations in Figure 6, the splitting of an ice floe moving past Fairway Rock, and ice movement along the shear zone west of Prince of Wales Shoal. Also note the turbulent wind wakes downstream of various landforms.

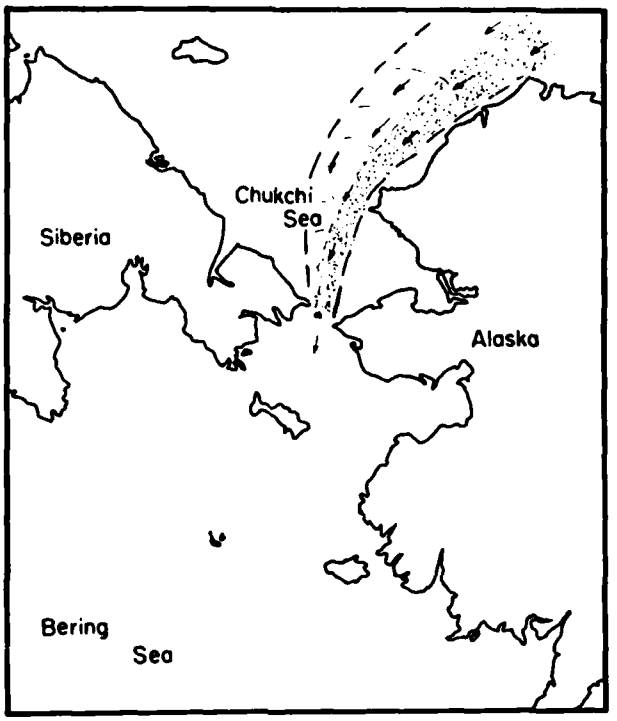

Figure 8. Area map of the Bering Strait. Dashed lines indicate zone of major ice stream which occurs during large southern ice drift. Stippled area is zone of maximum drift.

Figure 9. Two thick multi-year sea ice formations, center left in photo, and one thinner multi-year sea ice floe, near top center of photo, located off Tin City. Tin City is situated at the bottom on the south side of Cape Mountain (Fig. 3). Note shore ice pile-up on the terraced beach.

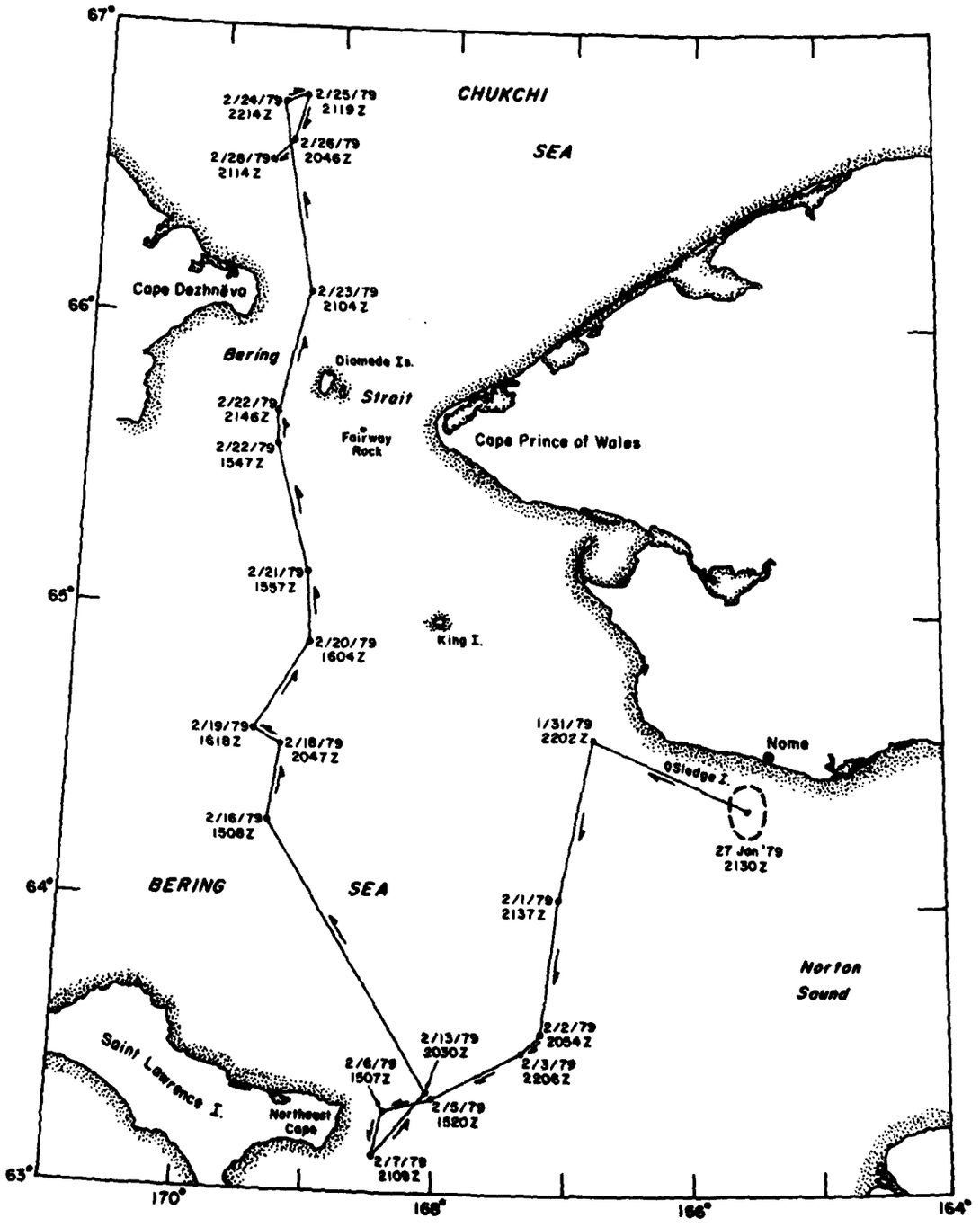

Figure 10. Ice field movement from Norton Sound into the Bering Sea and on into the Chukchi Sea from 27 Jan to 28 March 1979 (data source, Sea Ice Consultants, Camp Springs, Md.).

observed multi-year sea ice on the south side of King Island, offshore of Tin City (Fig. 9) and north of the Bering Strait.

A number of investigators have studied the Bering Strait ice breakout phenomenon and the magnitude of the forces needed to release the ice jam and allow the ice to flow southward through the constriction (Shapiro and Burns 1975, Sodhi 1977, Pritchard et al. 1979, Reimer 1979). Pritchard et al. (1979) found that if failure is caused by wind and current drag alone, i.e. neglecting any contribution from internal stress transmitted through the ice from distant locations, then an order of magnitude body force of 0.67 Pa is needed to collapse the arch. The assumptions are that the ice has a strength of 1.5×10^4 N m^{-1} and that failure occurs along a diamond-shaped yield surface.

In any event, once the Bering Strait ice arch collapses, in excess of 60,000 km^2 of sea ice from the Chukchi Sea can move southward at high velocities in a relatively short period of time (Ahlnas and Wendler 1979). Fairway Rock is situated in the center of the major ice floe stream through the strait.

Movement of ice northward through the Bering Strait is also driven by wind and current. Figure 10 shows the movement of an ice field tracked on satellite imagery by Sea Ice Consultants in February-March 1979 (unpublished data, courtesy W.S. Dehn). Between 27 and 31 January the ice field moved northwest with the strong coastal current out of Norton Sound. Thereafter, under changing wind fields, as depicted in Figure 11, the ice floes moved first southward to a location east of St.

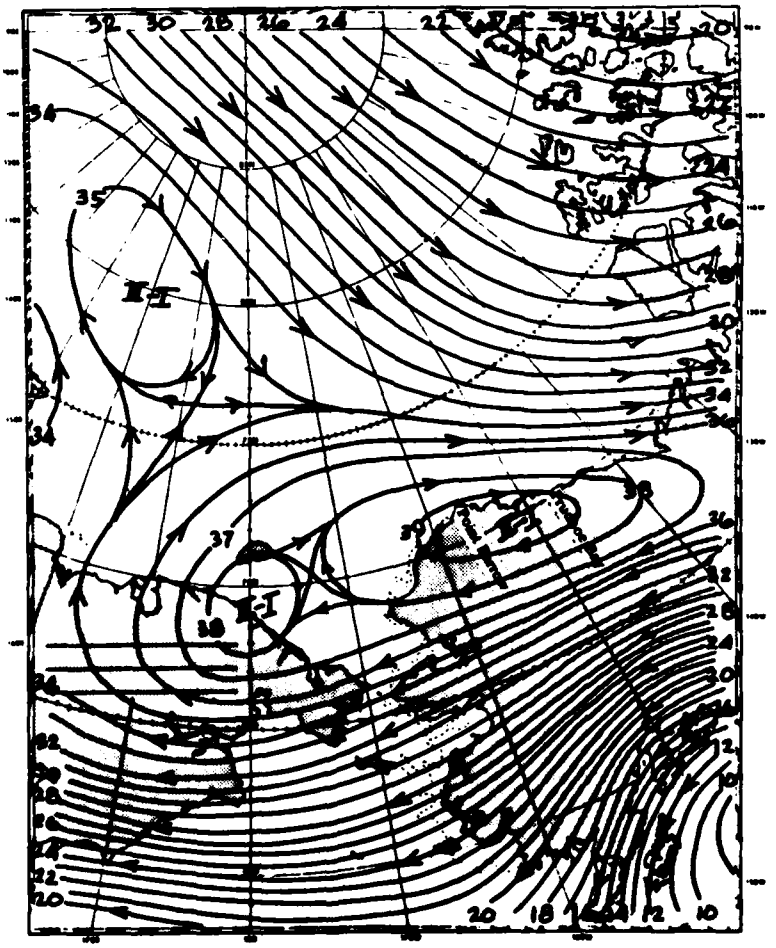

Figure 11. Fifteen-day mean sea level pressure composite charts. Arrows indicate wind direction. Numbers are pressure, e.g. 39 is 1039 millibars. The saddle area between the high pressure areas (H) is a zone of weak convergence and divergence (data source, Sea Ice Consultants, Camp Springs, Md.).

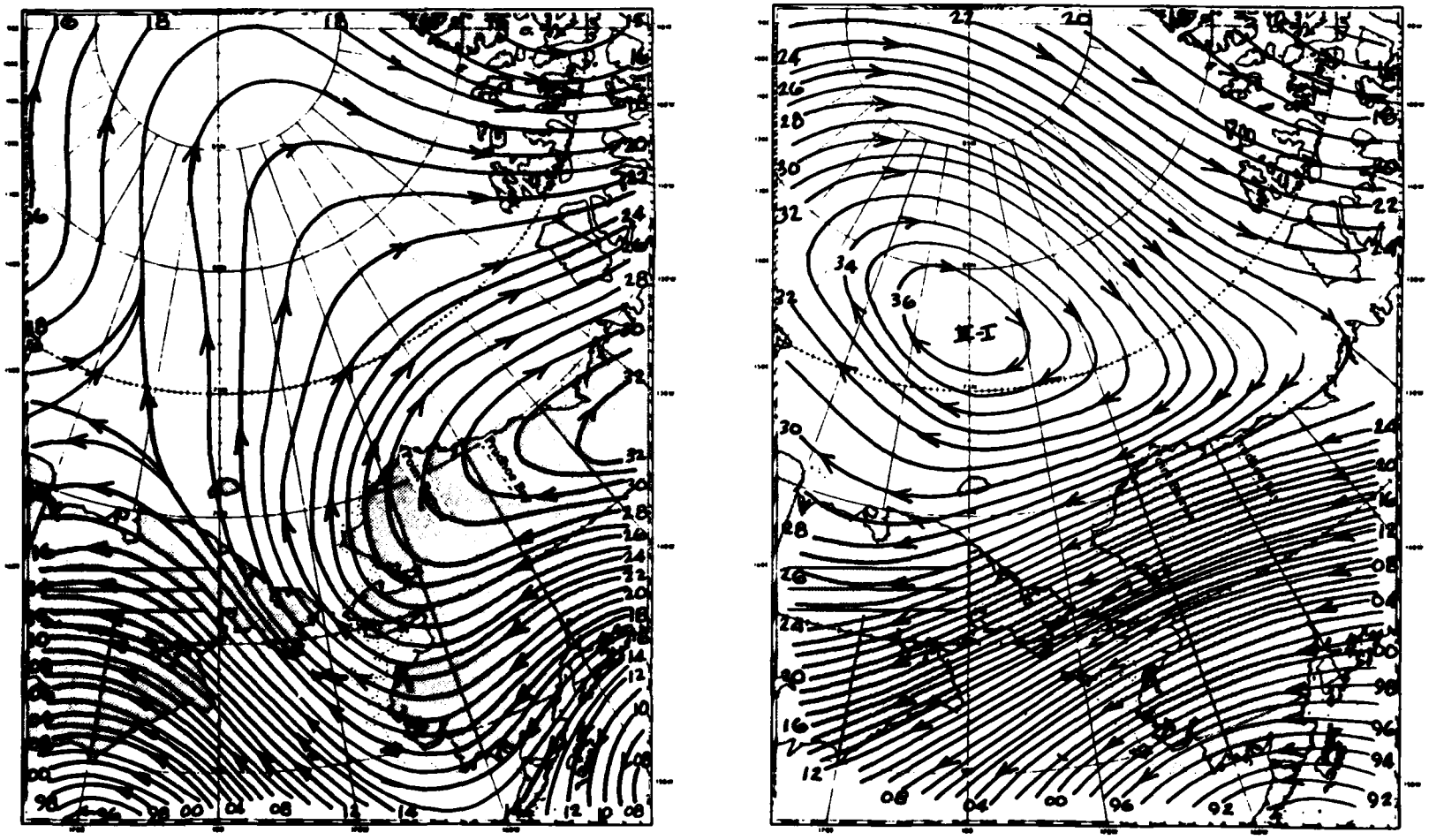

Second Half February (2/10/79-2/25/79)

First Half March (2/25/79-3/12/79)

Figure 11 (cont'd). Fifteen-day mean sea level pressure composite charts. Arrows indicate wind direction. Numbers are pressure, e.g. 39 is 1039 millibars. The saddle area between the high pressure areas (H) is a zone of weak convergence and divergence (data source, Sea Ice Consultants, Camp Springs, Md.).

Lawrence Island, and then northward through the Bering Strait. About 75 km north of the Bering Strait the floes changed direction again, first heading east and then southward. These ice floe movements are instructive for they represent one of the more complex routes which may be followed by petroleum introduced into the Norton Sound marine environment.

It is apparent that ice movement through the Bering Strait is both highly variable and quite dynamic. As a result, Fairway Rock is frequently impacted by either southerly- or northerly-moving ice floes throughout the winter season.

Figure 12. South side of Fairway Rock. Note low cloud ceiling.

FIELD RECONNAISSANCE

The 1980 field program consisted of two reconnaissances of the island in a small fixed-wing aircraft, during which hand-held camera photography and visual observations were made. One overflight in a remote sensing aircraft also obtained stereo aerial photography of the rock and portions of the ice rubble in the shear zone along Prince of Wales Shoal.

The first reconnaissance of Fairway Rock was made on 15 February 1980. The day was overcast, with a ceiling of about 150 m (Fig. 12). It was noted that the rock was surrounded by an icefoot with a very high "vertical" face. The piled-up ice appeared highly consolidated due to floes frequently pushing in against and shearing past the ice rubble which had formed during various north and south ice movement events. On the south side of the island a large ice floe was driven against the wall of the icefoot by the prevailing northward current flow (Fig. 12). To the north of the island was open water. At the base of the island on the north side, a large rock talus area was noted which upon first observation appeared to be ice rubble from a large ice ride-up event (Fig. 13).

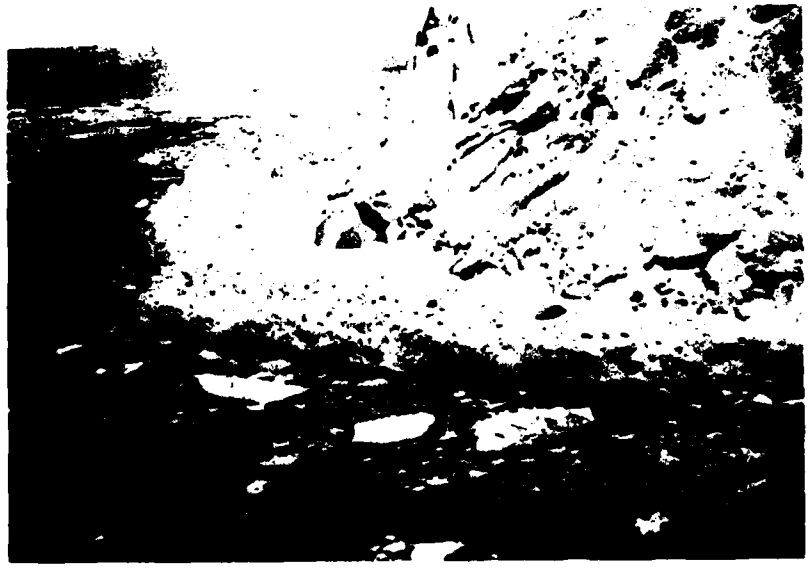

Figure 13. Morphology of icefoot on north side of Fairway Rock. Note rock talus area covered with snow.

a. 26 April 1980.

b. U.S. Naval photo of 8 April 1962.

Figure 14. South side of Fairway Rock.

Figure 15. West side of Fairway Rock.

Figure 16. North side of Fairway Rock.

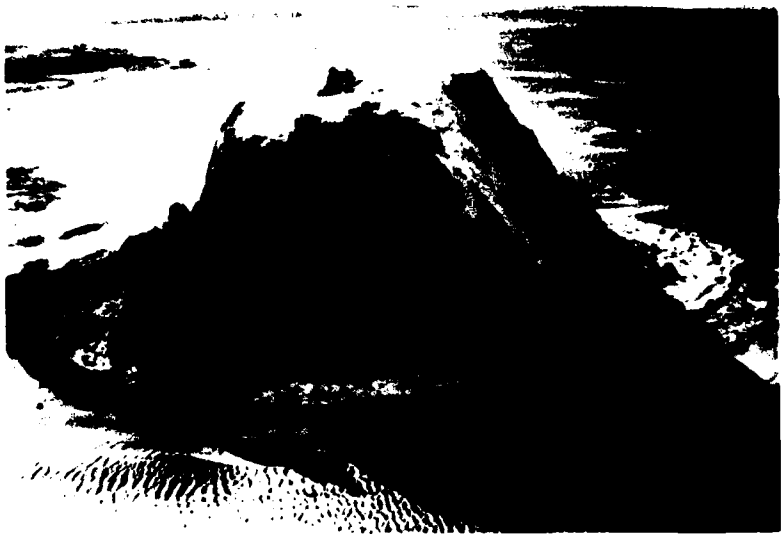

Figure 17. East side of Fairway Rock. Dark objects on top of island are large propane gas tanks and a generator installation.

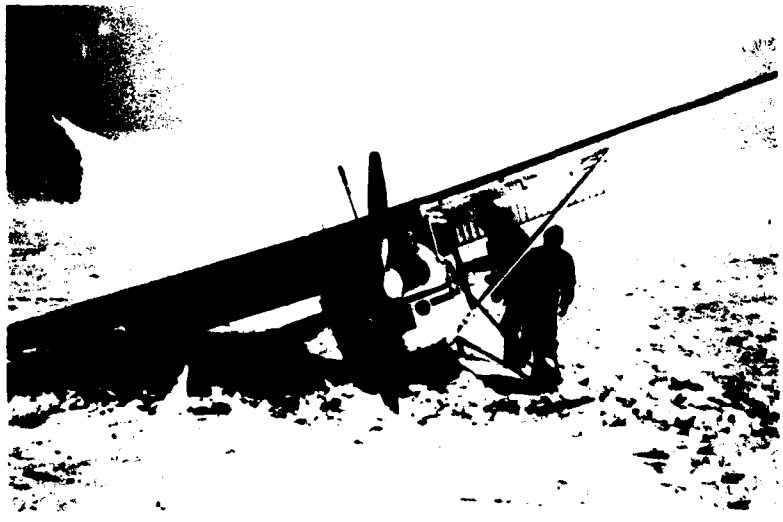

Figure 18. Termination of reconnaissance flight due to fuel loss through failed gas cap seal. (Landing gear destroyed, right wing tip bent, prop and stabilizer bent.)

The second reconnaissance was made on 26 April under a broken cloud cover. High winds and associated turbulence around the rock caused the small aircraft to be thrown around and prevented a close-up inspection of the icefoot. Nevertheless, the photos taken show an impressive accumulation of pressurized ice forming the icefoot, particularly on the north and south sides. At the time of the reconnaissance, open water surrounded the island. Off to the south significant open water and a diffused pack were noted, whereas to the north the pack ice could be seen in an apparent holding line between the Diomede Islands and Cape Prince of Wales. The northerly winds, while high, were not strong enough to drive the pack ice south against the prevailing southerly current.

A view of the south side of the rock is shown in Figure 14a. Note the steep face of the icefoot and the slope of the top of the island. A similar view of the rock taken on 8 April 1962 is shown in Figure

Figure 19. Aerial view over "south" side of Fairway Rock. Elevation profiles were made, from stereographic photo analysis, along the lines shown. North is to the right. (Photo was reduced to about 80% of original size; thus 0.8 in. = 333 ft.)

14b. A comparison of the icefoot in Figures 14a and 14b shows a remarkably similar icefoot configuration, indicating that yearly icefoot growth is controlled in part by submarine relief as well as by the general shape of the island. The ridged relief of the southern and northern portions of the icefoot can be seen from the west in Figure 15. The northern half of the island is seen caked with snow, and along the base the rock surface is covered with a layer of glaze and spray ice. This is again apparent in a view from the north (Fig. 16). In this photo the large rock talus area is visible, as is the shear face of the massive icefoot. An east view of the rock (Fig. 17) shows portions of the vertical rock face at sea level and thick icing accumulations covering the rock to an apparent height in excess of 40 m above sea level.

Following the flyby of Fairway Rock, a reconnaissance of pressure ridge features within the shear zone west of Prince of Wales Shoal and of

Figure 20. Aerial view over "north" side of Fairway Rock. North is to the right. (Photo was reduced to about 80% of original size; thus 0.8 in. = 333 ft.)

ice rubble piles on the shoal was planned. However, an engine malfunction and a short (30-m) two-bounce sideways forced landing (Fig. 18) precluded accomplishment of this objective.

Aerial photography of Fairway Rock and portions of the Cape Prince of Wales shear zone was obtained on 14 March 1980. Two views of Fairway Rock are shown in Figures 19 and 20. The ridge systems composing the southern icefoot are quite apparent due to the favorable sun angle. The general bluntness of the icefoot is striking, as is the narrow width of the icefoot on the west and southeast sides of the rock. In these areas the rock wall seems to drop vertically into the sea. Unlike the view of the rock shown in Figure 10 the south face of the rock at this time was caked with snow and/or ice. The top of the rock is clearly windswept; visible are shadows from a cluster of propane tanks and a small generator used to power salinity, temperature, conductivity and current instruments on the sea bottom (G. Bloom, pers. correspondence).

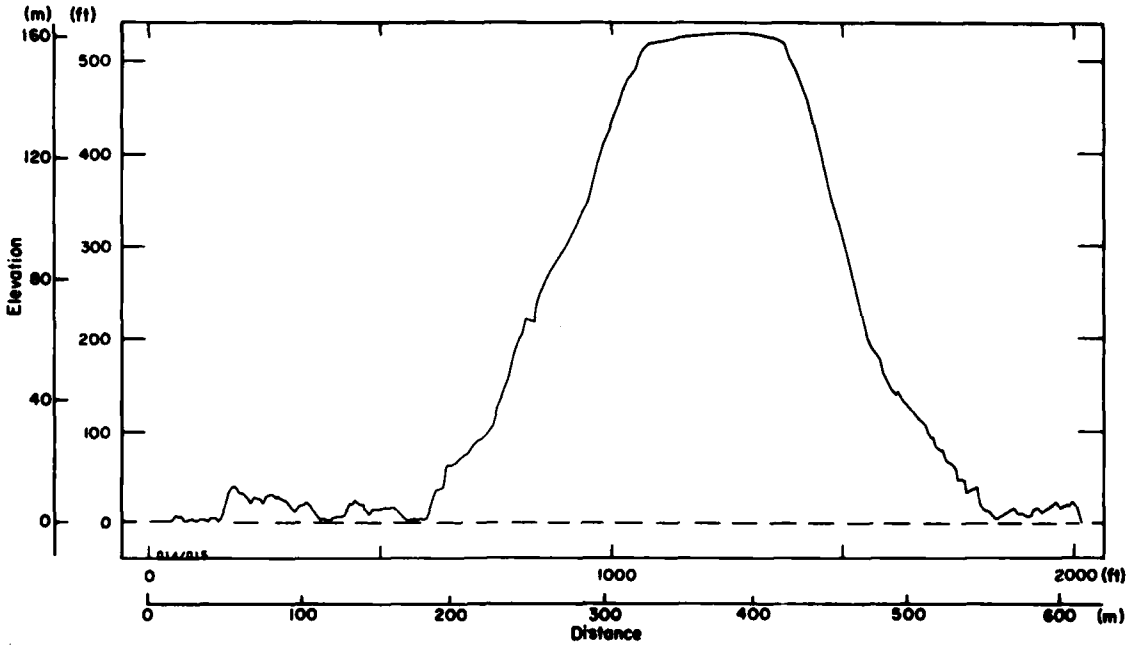

Figure 21. Elevation profile of icefoot and Fairway Rock along line 1A.

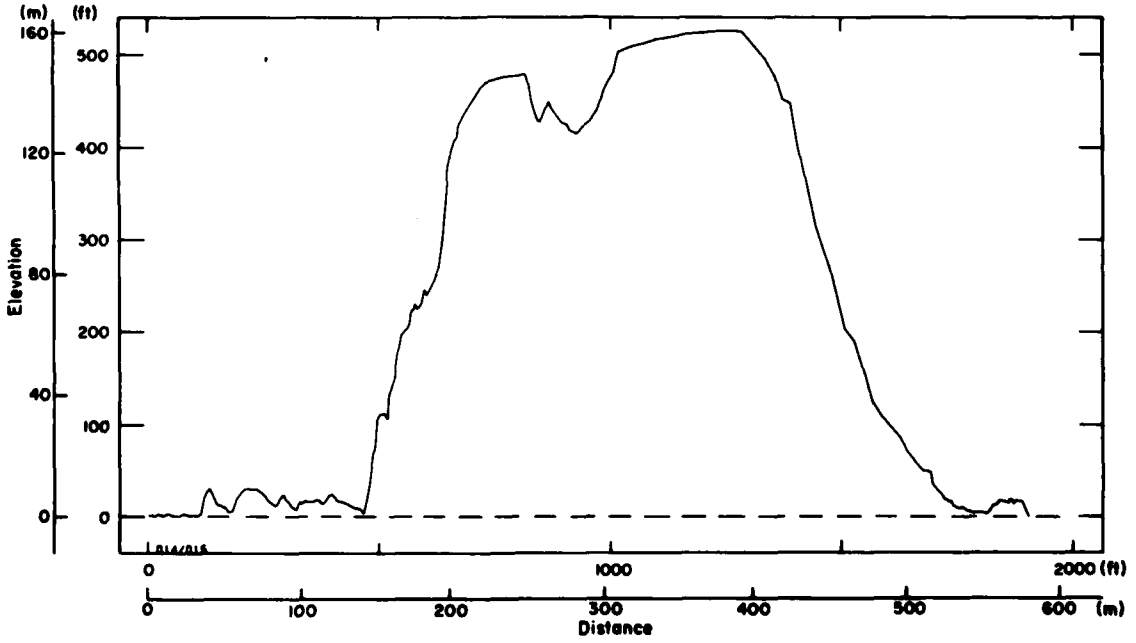

Figure 22. Elevation profile of icefoot and Fairway Rock along line 6F.

Elevation profiles of the ice rubble surrounding the island were made from stereopairs. The profile lines are drawn and numbered in Figure 19. The elevation profiles are presented in Figures 21–28. These profiles reveal that the icefoot attains an elevation of at least 14.6 m, has a steep slope in excess of 70° on the seaward side, and in places rests against an apparently near-vertical rock wall. Calculated interior ridge slope angles averaged 33°.

Field measurements of free-floating first-year pressure ridges have shown that their sail height to keel draft ratio is of the order of 1 to 4.5 (Kovacs

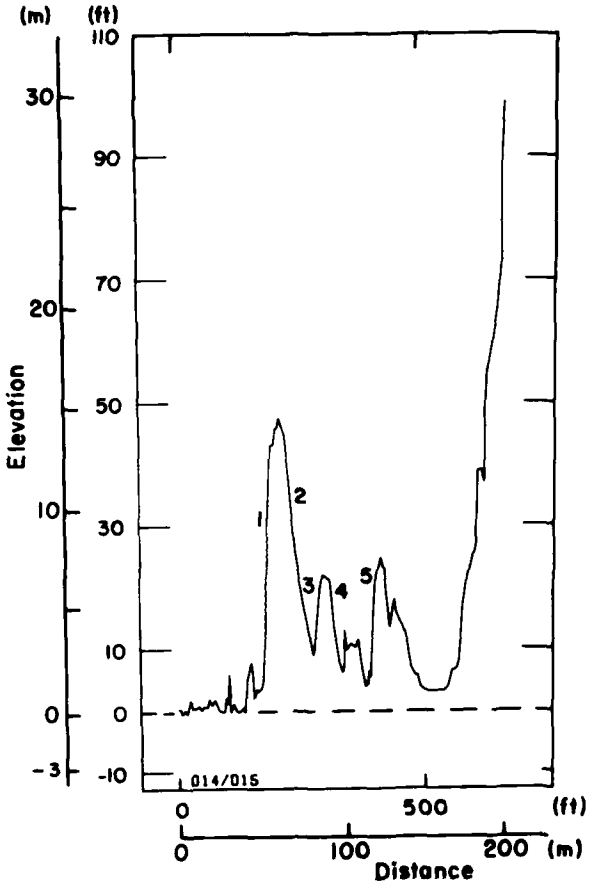

Figure 23. Fairway Rock—icefoot profile 2B. Ice ridge slopes 1 through 5 are 73, 30, 35, 37 and 38 degrees, respectively. Highest point on icefoot is 14.7 m.

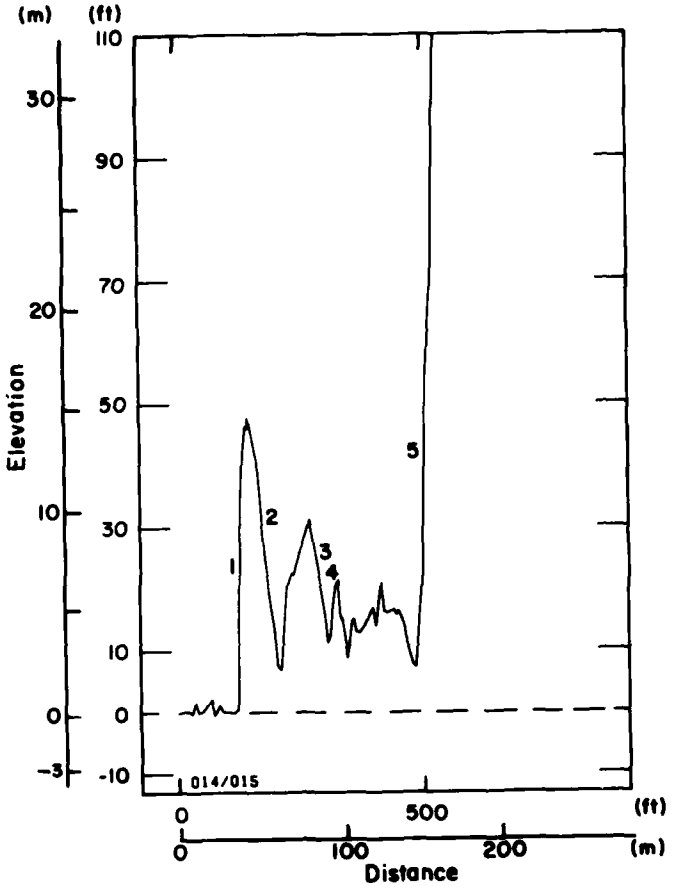

Figure 24. Fairway Rock—icefoot profile 3C. Ice ridge slopes 1 through 4 are 70, 35, 28 and 29 degrees respectively and the rock face slope at 5 is 76 degrees. Highest point on icefoot is 14.7 m.

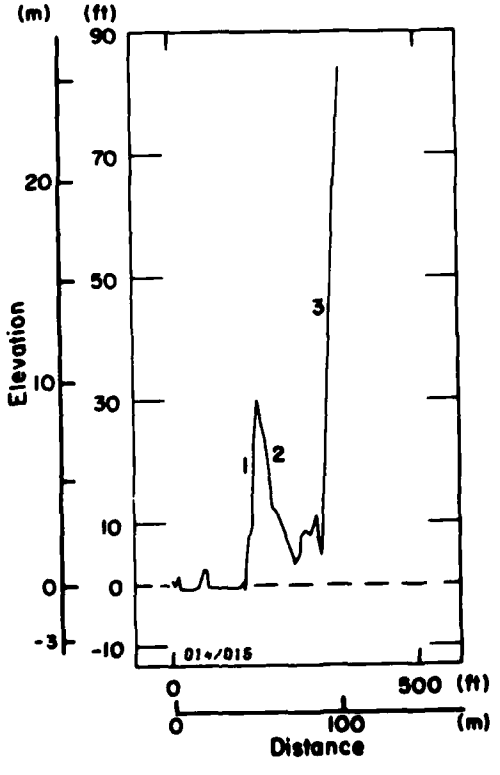

Figure 25. Fairway Rock—icefoot profile 4D. Ice ridge slopes 1 and 2 are 77 and 30 degrees respectively and the rock face slope at 3 is 62 degrees. Highest point on icefoot is 9.4 m.

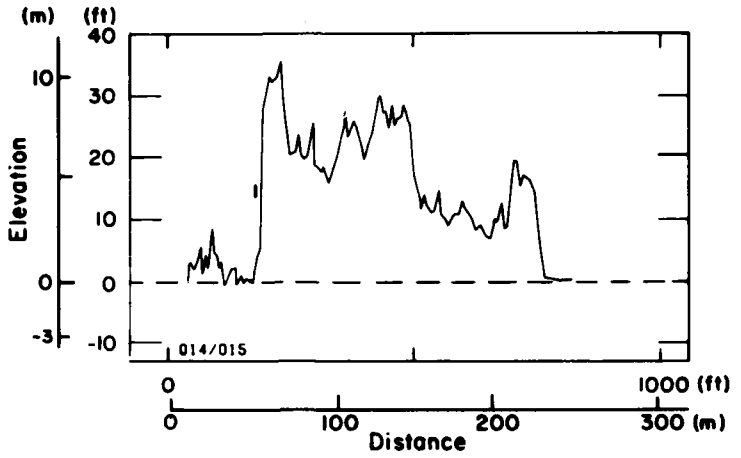

Figure 26. Fairway Rock—icefoot profile 5E. Ice ridge slope 1 is 76 degrees. Highest point on icefoot is 11.1 m.

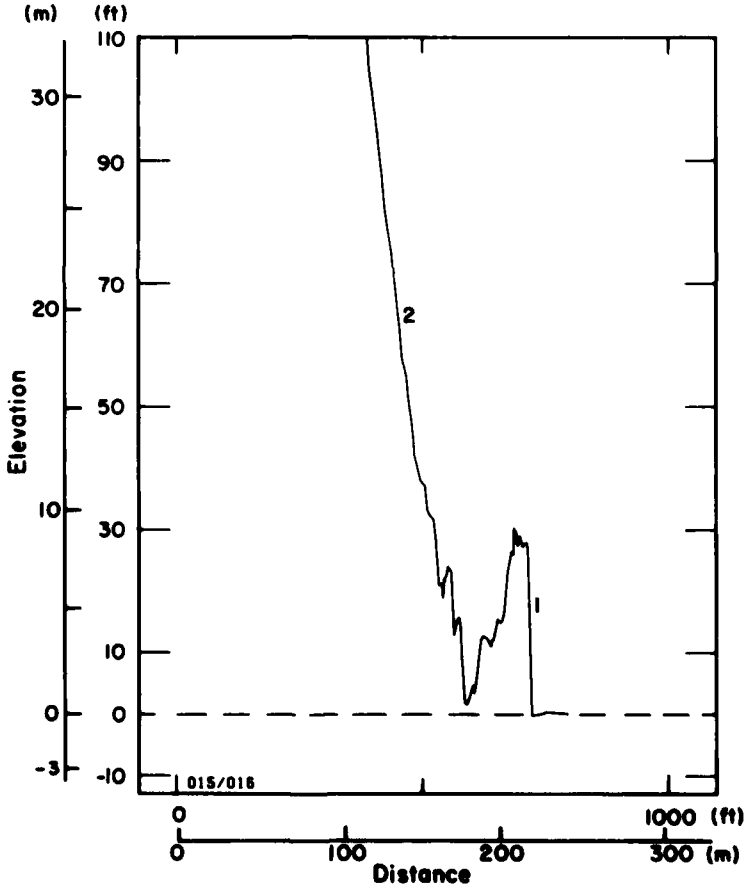

Figure 27. Fairway Rock—icefoot profile 7G. Ice ridge slope 1 is 73 degrees and rock face slope at 2 is 50 degrees. Highest point on icefoot is 9.6 m.

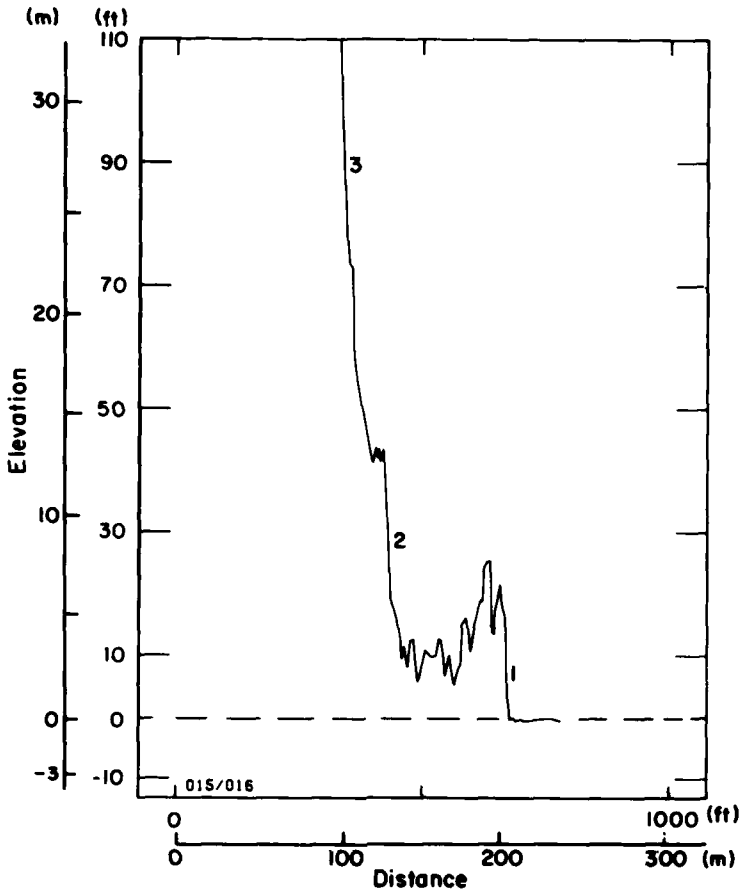

Figure 28. Fairway Rock—icefoot profile 8H. Ice ridge slope 1 is 72 degrees and rock face slopes 2 and 3 are 66 and 64 degrees respectively. Highest point on icefoot is 8.0 m.

and Mellor 1974). If the 14-m-high ridges composing the icefoot at Fairway Rock were free-floating it could be assumed that their keels would extend downward to the 63-m depth. Since the water depth surrounding Fairway Rock is at least 10 m shallower than this, and given the fact that boulder talus composing much of the submarine rock face slopes gradually outward with depth (Fig. 2), it is only reasonable to conclude that the icefoot is firmly grounded. It is assumed that ice which is not securely grounded is rapidly dislodged by pack ice forces generated during major north or south ice movement events.

In April 1981 an investigation of the Fairway Rock icefoot sail and keel and the submarine slope of the rock was planned from the U.S. Coast Guard icebreaker *Polar Sea*. However, because this ship became disabled in the ice of the Chukchi Sea, our field program was reduced to a short inspection using a helicopter.

Aerial views of Fairway Rock taken during our April 1981 visit are shown in Figure 29. The north side of the rock is again seen to be covered with ice and snow, and the shape of the icefoot is consistent with previous observations. A surface view of position one in Figure 29 is shown in Figure 30. The ice floe on which we landed was relatively stationary during our visit, but on the west side of the island the ice was moving briskly northward with the current. The icefoot wall on the left in Figure 30 was measured to be 16.5 m high and was found to be near vertical. A view of the ice rubble looking west from the top of this high wall is shown in Figure 31. The numbers on this photo correspond to those at the locations shown in Figure 29b. Bear tracks were noted in the snow alongside the island and the ice rubble. A walk to the west side of the island ended where the icefoot became about a meter wide and the rock wall dropped "vertically" into the sea, position 5 in Figure 29.

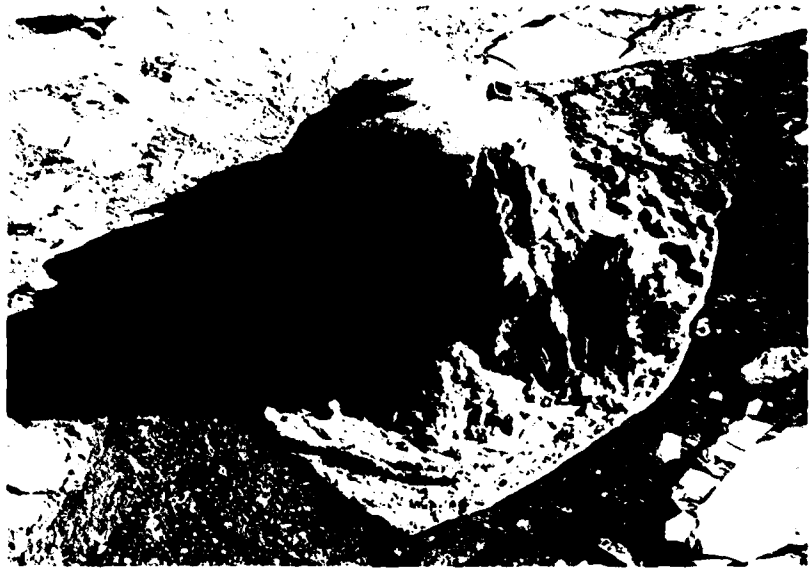

a. North.

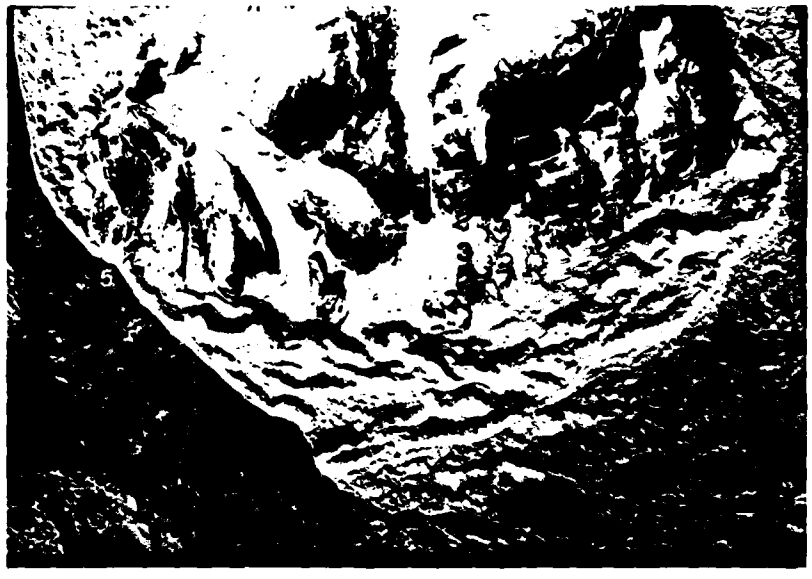

b. South.

Figure 29. Fairway Rock icefoot, April 1981.

Following our Fairway Rock stop we visited Little Diomede Island. The south and east sides of this island were also found to be surrounded by a massive icefoot (Fig. 32). On the north side of the island the rock surface up to 10 m above sea level was found to be coated with up to a 0.3-m-thick icing (Fig. 33). The icing, while decreasing in thickness with elevation, did extend to the top of the island (Fig. 34).

Three aerial views of the rubble fields located in the shear zone west of Prince of Wales Shoal are shown in Figure 35. These shear ridge fields are not as massive as some which have been observed farther north near the Arctic Circle (Kovacs 1972). Nevertheless, they are large, and because they formed under shear-compression can be assumed to be reasonably compact. These features would pose a major obstacle to winter navigation. On oc-

Figure 30. Icefoot on southeast side of Fairway Rock.

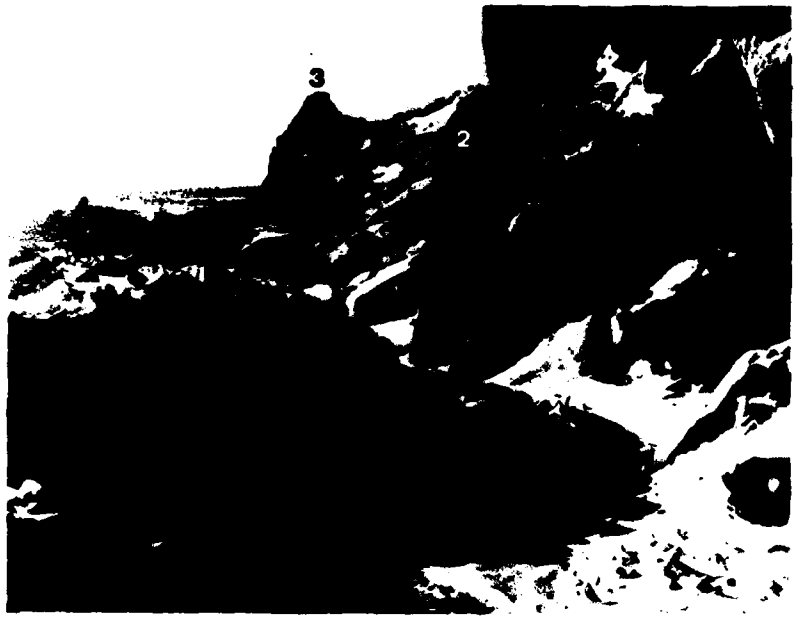

Figure 31. Icefoot rubble along south side of Fairway Rock.

Figure 32. Icefoot on southeast side of Little Diomede Island. Big Diomede Island is in the background.

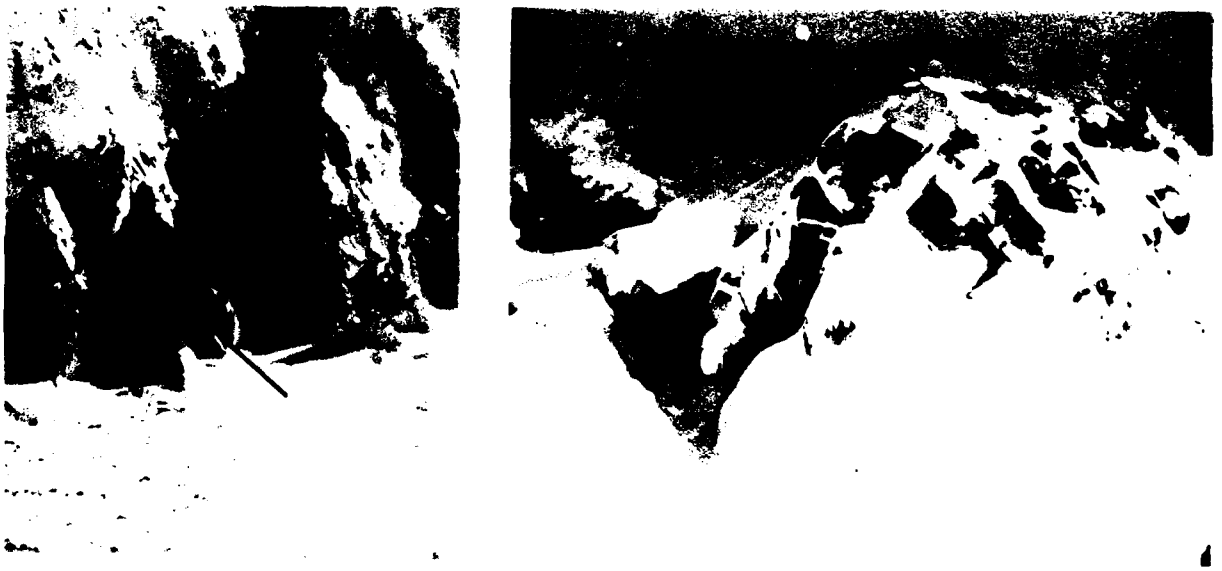

a. Aerial view.

b. Ground view of position indicated by arrow in (a).

Figure 33. Icing on north side of Little Diomede Island.

Figure 34. Icing on rock surface at the top of Little Diomede Island.

casion these formations are dislodged and driven southward. They therefore represent one of the major ice features to be considered in the design of a structure to be placed in the northern Bering Sea. The high points on elevation profiles 30–37 shown in Figures 36–43 are 5.7, 5.8, 4.4, 4.1, 4.5, 5.9, 4.2 and 4.8 m respectively. While the elevation profiles reveal shear ridge ice relief of over 5 m, ridges on the order of 3 m high are more typical.

Rubble field profiles were constructed from elevation data obtained from stereographic photo analysis where all ridge peak and trough elevations were determined along a profile. Among these features additional elevation determinations were made at random to provide representative intermediate ice relief. Typically, each profile comprised between 100 and 180 data points. This translates into one data point about every 5 m. Thus, there is a paucity and uneven distribution of elevation data along each profile. Nevertheless, to obtain a general idea of the ice thickness in the rubble fields, the data were analyzed to determine the root mean square (RMS) elevation for each profile by:

$$\text{RMS} = \sqrt{\frac{h_1^2 + h_2^2 + h_3^2 \ldots h_n^2}{n}}$$

where h = individual ice elevation and n = number of data points.

From this analysis the RMS elevations for profiles 30 through 37 were found to be 2.53, 2.07, 2.23, 2.16, 2.12, 1.93, 1.48 and 1.79 m respectively. The average of these RMS values is 2.0 m. Using a 1:4.5 sail height to keel depth ratio for first-year pressure ridges (Kovacs and Mellor 1974) we can deduce an RMS ice thickness of 11 m. While the analysis is limited by the data, as previously mentioned, and by the fact that some rubble profiles include short segments of undeformed ice, it does give some indication of the relative ice thickness in the rubble fields.

In early April 1982, we briefly visited Fairway Rock by helicopter and made the observation given in Appendix A.

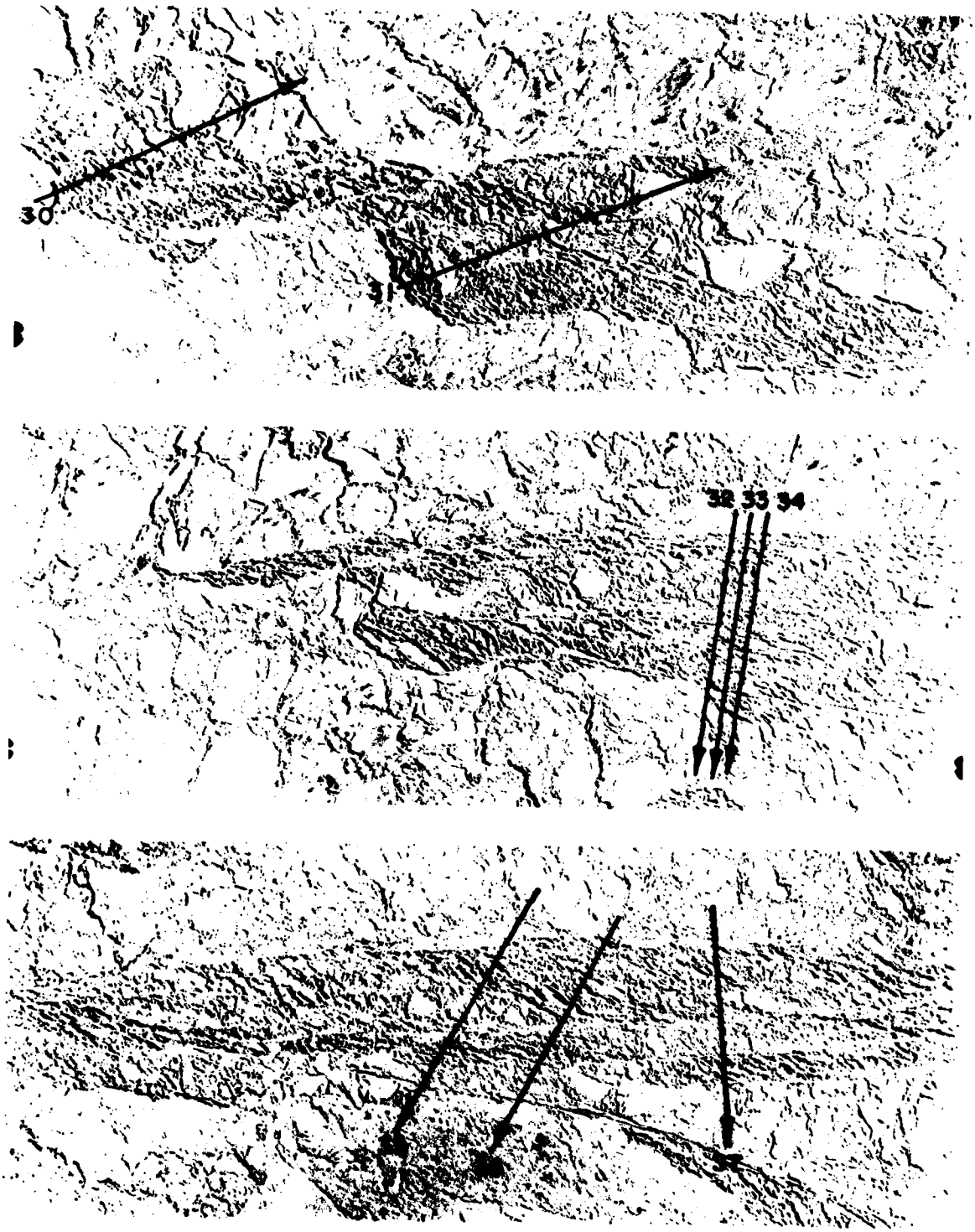

Figure 35. Aerial views of shear ridge fields west of Prince of Wales Shoal. Numbered lines represent sites of elevation profiles in Figures 36-43. North is to right.

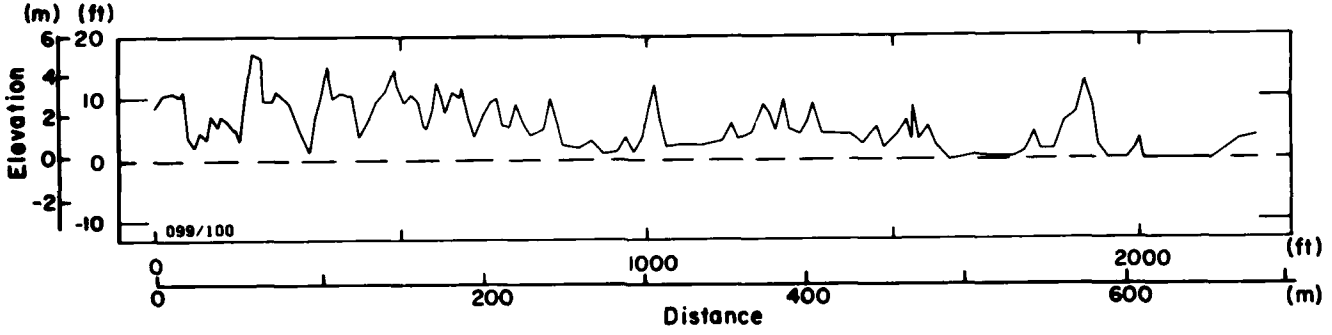

Figure 36. Shear ridge field profile 30.

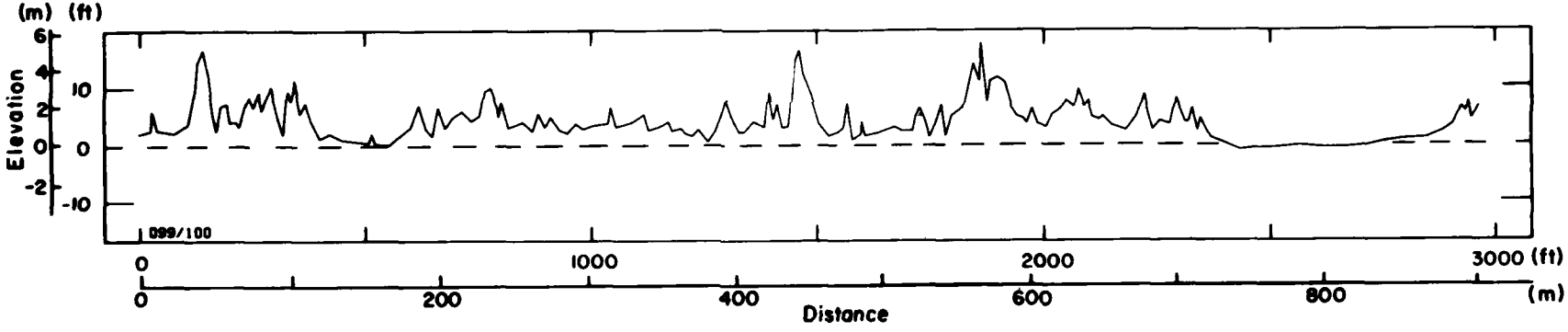

Figure 37. Shear ridge field profile 31.

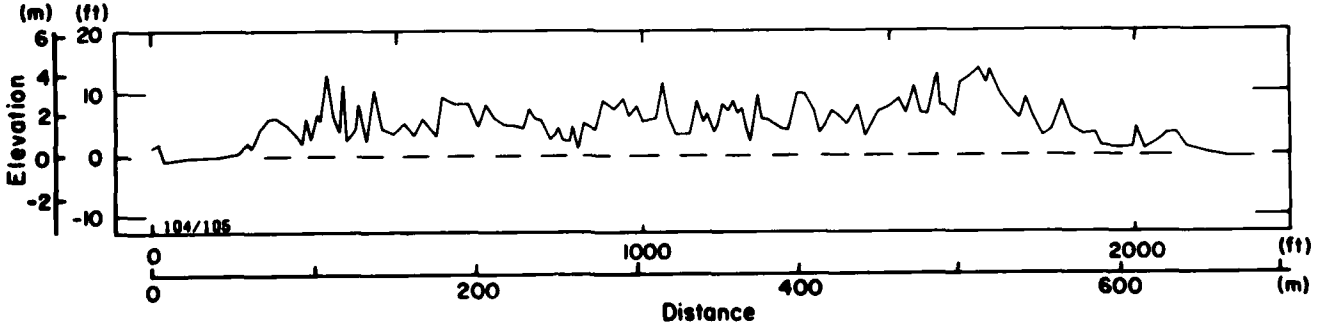

Figure 38. Shear ridge field profile 32.

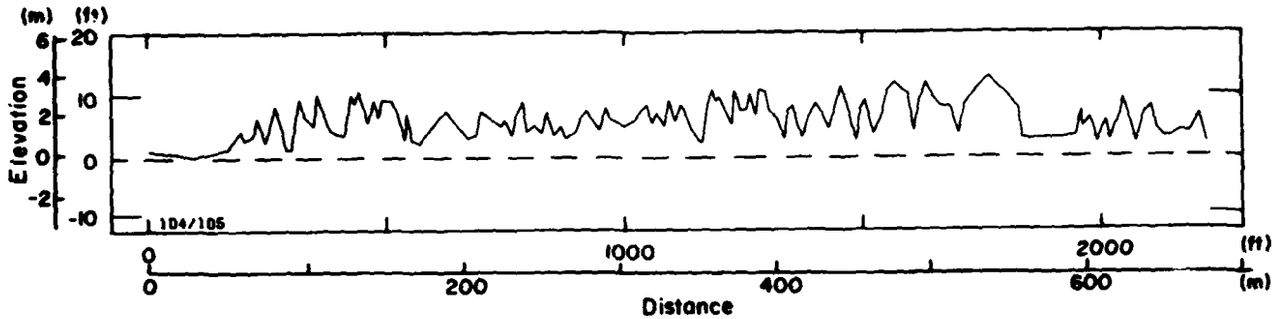

Figure 39. Shear ridge field profile 33.

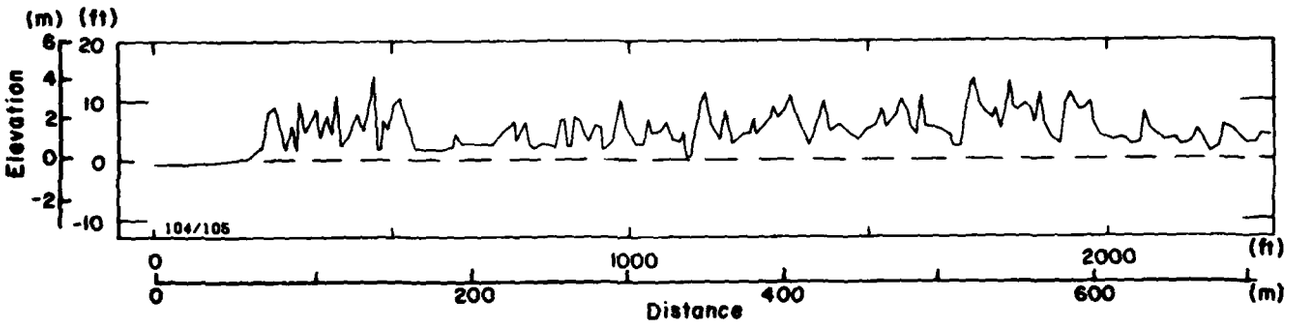

Figure 40. Shear ridge field profile 34.

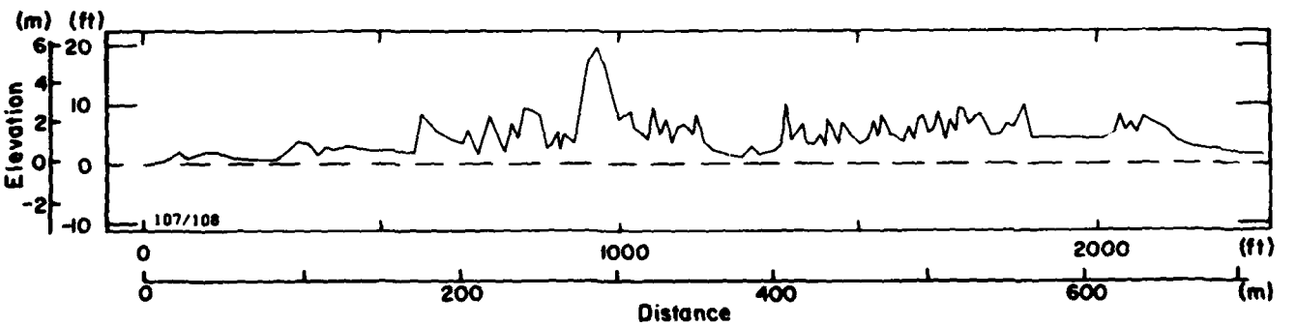

Figure 41. Shear ridge field profile 35.

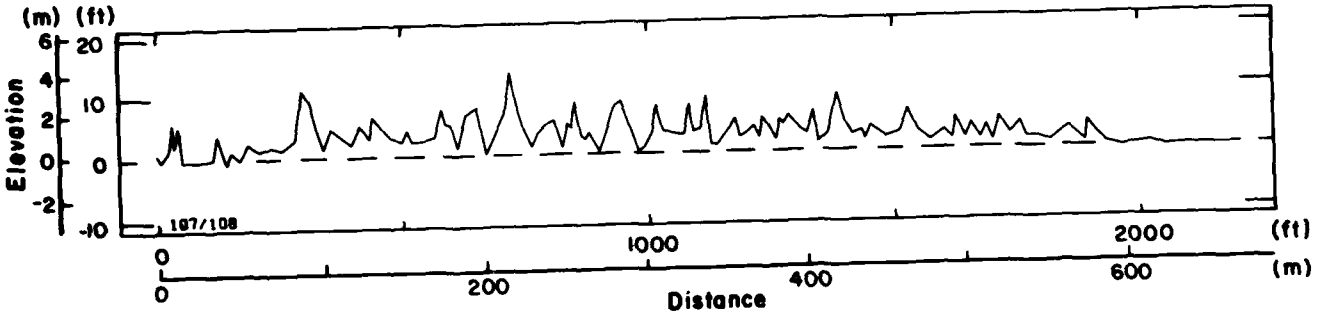

Figure 42. Shear ridge field profile 36.

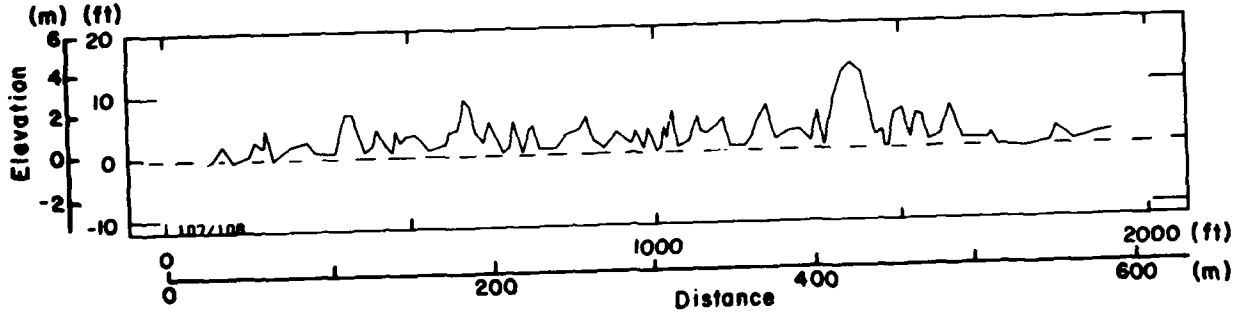

Figure 43. Shear ridge field profile 37.

ESTIMATION OF ICE FORCES ON FAIRWAY ROCK

An estimate of the ice forces against Fairway Rock was made based on limited observations of the icefoot and the elevation of ice pile-ups as revealed by stereographic photo surveying. The magnitude of the ice forces is dependent upon the mode of ice-island interaction and available forces. Five ice failure modes were considered and an estimate of the available forces is given below.

1. Creep Deformation

Under situations where the ice is moving slowly against Fairway Rock and all the ice deformation is by creep, an estimate of the total ice load on the rock can be obtained by applying the reference stress concept. This technique gives approximate solutions to non-linear structural problems by combining the simpler linear-elastic and rigid-plastic problems. Ponter et al. (1981) have successfully applied reference stress theory to low velocity ice indentation problems. For a vertical, flat indentor, the reference stress theory gives

$$F = \eta D t F_\sigma \left[\frac{V_i/D}{\eta\psi}\right] \qquad (1)$$

where F = total ice force
D = structure width (~400 m for Fairway Rock)
t = ice thickness
V_i = ice velocity
$F_\sigma[x]$ = uniaxial stress corresponding to a uniaxial strain-rate x
η and ψ = functions of D/t derived from a solution to the plastic and corresponding elastic edge indentation problems, respectively.

In plane stress, where $D >> t$ and there is free slip between the ice and structure,

$$\eta = \frac{2}{\sqrt{3}}\left[1 + \frac{\sqrt{2}}{2}\left(\frac{t}{D}\right)^{1/2} + \frac{1}{4}\left(\frac{t}{D}\right)\right]$$

and

$$\psi = 0.441.$$

If we assume an upper bound ice velocity of 5×10^{-3} m/s for this case, and sheet ice thicknesses of 0.5, 1.0 and 1.5 m, we can estimate the total "creep" ice load on the rock from the reference strain-rate and the corresponding uniaxial compressive strength determined from the laboratory tests. Tabulated values are given in Table 1. The uniaxial compressive strength of the ice at the reference strain-rate was obtained from laboratory data for sea ice presented by Wang (1979). Ice pressure on the rock for an ice velocity of 5×10^{-3} m/s is about 1.60 MPa (235 psi). Similar results are obtained from the plane stress case where there is no slip between the ice and structure. It is interesting to note that the reference strain rate as determined by theory is about $V_i/0.5D$ as compared to the less conservative, semi-empirical values of $V_i/2D$ and $V_i/4D$ used by Ralston (1979) and Michel and Toussaint (1976), respectively. The theoretical reference strain-rate is probably more appropriate at low ice velocities.

2. Crushing Failure

The potential ice force due to the crushing of an ice sheet against the "vertical" faces of the rock or the icefoot rubble pile may be calculated from the Korzhavin formula (Croasdale 1980):

$$F = Imk\sigma_c Dt \qquad (2)$$

where F = total ice force
k = factor to account for the lack of uniform ice contact
I = indentation factor, $I = 2.5$ for narrow structure, $I = 1$ for wide structure

Table 1. Calculated creep ice loads for an ice velocity of 5×10^{-3} m/s and different ice thicknesses.

Ice thickness (m)	Ice thickness (in.)	η	$V_i/D/\eta\psi$ (s^{-1})	Ice strength (MPa)	Ice strength (psi)	Ice load (MN)	Ice load (lb)
0.5	19.7	1.155	2.45×10^{-9}	1.4	203	325	7.31×10^7
1.0	39.4	1.156	2.45×10^{-9}	1.4	203	650	1.46×10^8
1.5	59.1	1.156	2.45×10^{-9}	1.4	203	975	2.19×10^8

m = shape factor, m = 1 for circular structure
σ_c = uniaxial compressive strength
D = structure width (about 400 m in the case of Fairway Rock)
t = ice thickness.

The values for m and I are taken to be 1 because $D/t \gg 1$. The contact factor k accounts for the non-simultaneous failure of the ice sheet across the entire structure width. Kry (1978) presented a statistical study in which the variation of the stresses with respect to ice displacement is shown to be reduced due to non-simultaneous failure action. Thus, the effective stress for a wide structure is less than the peak stress for a narrow structure. Although there are no recommended or suggested values of k for a wide structure, a low value of 0.4 has been suggested by Korzhavin for fast-moving floes (Michel 1970).

The selection of a compressive strength for the ice is a difficult task, as it depends upon so many parameters, such as ice temperature, salinity, grain size, crystallographic structure, strain rate, etc. In the Arctic, the average temperature of sea ice is about -10°C, and we may use the laboratory σ_c data determined at -10°C.

Michel and Toussaint (1976) have proposed an empirical definition of strain rate as $\dot{\epsilon}_{eff} = V_i/4D$, where V_i is the velocity of ice, and D the structure width. This definition of strain rate is slightly more unconservative than that proposed by Ralston (1979), $\dot{\epsilon}_{eff} = V_i/2D$, and that of the reference stress theory. However, using a denominator of $4D$ gives better agreement between uniaxial compression and indentation tests at moderate strain rates. The strain rate for V_i = 0.5 m/s and D = 400 m is $\dot{\epsilon}_{eff} = 3.1\times10^{-4}$. Using the compressive strength of sea ice at this strain rate as given by Wang (1979), the crushing strength of ice is found to be on the order of 4830 kPa (700 psi). Substituting these values into eq 2, we have $p = F/Dt = Imk\sigma_c$ = 1930 kPa (280 psi). The total force is given by $F = pDt$, and it is estimated to be 385 MN (85×10^6 lb), 770 MN (170×10^6 lb) and 1160 MN (255×10^6 lb) for 0.5-, 1.0- and 1.5-m-thick ice sheets, respectively.

3. Flexural Failure

The following formula can be used to calculate the ice forces on a sloping wide structure (Croasdale 1980):

$$\frac{H}{b} = \sigma_f\left(\frac{\varrho_w g t^3}{E}\right)^{0.25} C_1 + Zt\varrho_i g C_2 \qquad (3)$$

where H = horizontal force required to break and push the ice sheet up
b = ice sheet width
σ_f = ice flexural strength
t = ice thickness
E = ice modulus of elasticity
ϱ_w = water density
ϱ_i = ice density
Z = height reached by ice on the slope
g = acceleration due to gravity
C_1, C_2 = factors which depend on slope angle α and coefficient of friction, μ, as obtained from Figures 44 and 45.

The slope of the beach (if there is any at Fairway Rock) is not known; however, taking α = 33° (average measured ice pile-up slope angle), μ = 0.3, σ_f = 700 kPa (100 psi), $E = 10^6$ kPa (1.45×10^5 psi), ϱ_w = 1030 kg/m³ (64.3 lb/ft³), ϱ_i = 920 kg/m³ (57.43 lb/ft³), Z = 15 m (49.21 ft), we get the values of H/b shown in Table 2 for different thicknesses of ice.

As can be seen from the values in the above table, the force required to push the ice blocks up the ice pile-up slope constitutes the major portion of the force per unit width. The ice pile-ups may reach 15 m high but are certainly not this high everywhere. Therefore, the estimates given are considered to represent an upper value. In addition, because flexural failure is not expected to occur simultaneously across the entire width of the rock, the above breaking force values would be in-

Table 2. Values of H/b.

Ice thickness		Force/width to push ice upslope		Total force/width H/b		Pressure P	
(m)	(in.)	(kN/m)	(lb/ft)	(kN/m)	(lb/ft)	(kPa)	(psi)
0.5	19.7	149	10,204	161	11,057	322	46.8
1.0	39.4	298	20,408	327	22,436	327	47.5
1.5	59.1	447	30,612	591	40,488	394	57.13

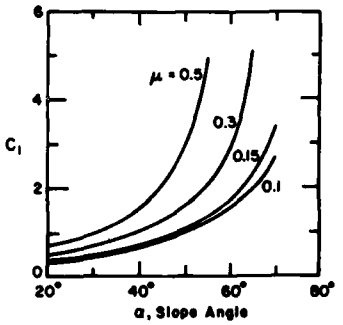

Figure 44. Coefficient C_1 versus slope angle and friction (after Croasdale 1980).

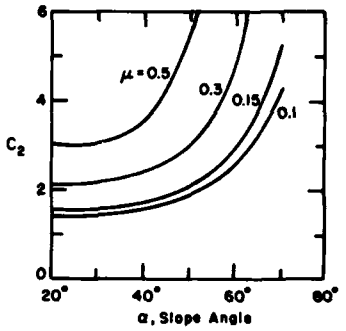

Figure 45. Coefficient C_2 versus slope angle and friction (after Croasdale 1980).

appropriate to apply uniformly across the entire face of the island or the icefoot.

4. Forces Required to Form Floating or Grounded Pressure Ridges Along the Rock or to Pile Ice on the Beaches

The average force required to form a floating or a grounded pressure ridge (Fig. 46a, b) can be obtained by considering the force required to add gravitational potential energy to the ice pile and to overcome ice block friction as discussed by Parmerter and Coon (1973) and Kry (1977). In a similar manner, the force required to add gravitational potential energy to a shore ice pile-up (Fig. 46c) was discussed by Kovacs and Sodhi (1980). The equations for calculating the force F required to

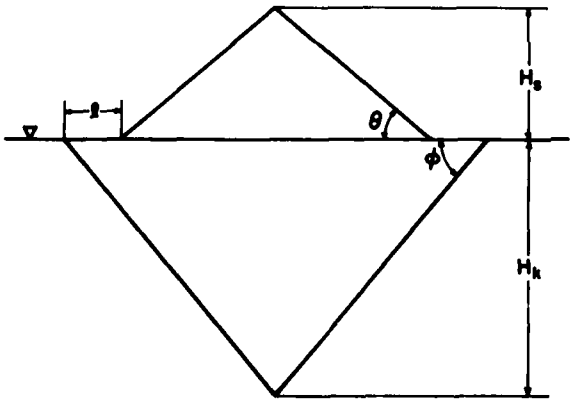

a. Model for floating pressure ridge.

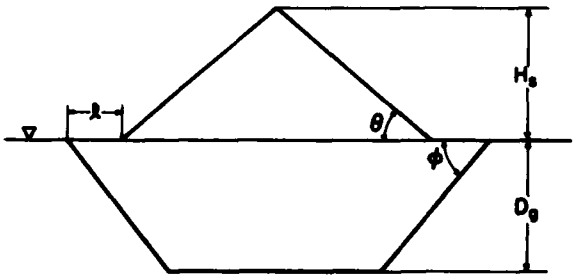

b. Model for grounded pressure ridge.

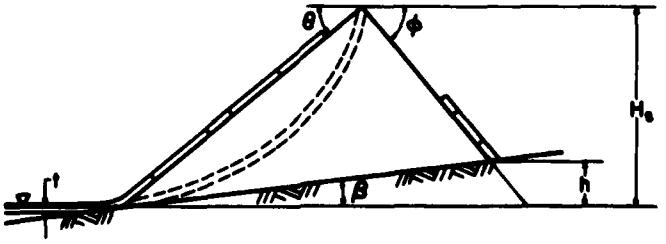

c. Model for shore ice pile-up.

Figure 46. Sea ice pressure ridge and shore ice pile-up models.

add gravitational energy to a floating ridge (fl), a grounded ridge (gr), and a shore ice pile-up (pl) are as follows:

$$F_{fl} = \frac{1}{2}\,\varrho_i g H_s t \tag{4}$$

$$F_{gr} = \frac{1}{2}\,\varrho_i g H_s t \left[\frac{\varrho_w - \varrho_i}{\varrho_i}\left(\frac{D_g}{H_s}\right)^2 + 1\right] \Big/ \left(\frac{D_g}{H_s} + 1\right) \tag{5}$$

$$F_{pl} = \alpha\frac{1}{2}\,\varrho_i g H_s t \tag{6}$$

where F = force per unit width
ϱ_i = ice density
g = acceleration due to gravity
H_s = ridge sail height or height of ice pile
t = ice thickness
ϱ_w = water density
D_g = ridge keel grounded depth
α = a factor whose value ranges from 1 (for a pile-up on level ground) to 2 (for an ice ride-up).

It can be shown that $F_{gr} < F_{fl}$ because $D_g/H_s < (\varrho_i/\varrho_w - \varrho_i)$ (Kry 1977). The maximum force per unit width is therefore due to ice pile-up or ride-up.

The frictional forces (F_{fr}) per unit width of an ice sheet required to push through a rubble pile (Fig. 46c) may be estimated by the following expression (Kovacs and Sodhi 1980, Kry 1980):

$$F_{fr} = \mu_i(1-\gamma)\,\varrho_i g f H^2 \cot\theta \tag{7}$$

where μ_i = coefficient of friction of ice on ice
γ = porosity of the sail
f = fraction of the sail mass that acts to create the frictional force
H = height of sail or pile-up
θ = slope angle of sail or pile-up from the horizontal.

The combined forces to add gravitational energy and to overcome frictional forces in an ice rubble are of the same order of magnitude as that required for flexural failure of an ice sheet against a sloping surface.

5. Buckling Failure

When an ice sheet moves against a wide structure or a beach, it is generally considered to fail in a mode which requires the least force. In the previous three sections, the average ice pressures required to fail an ice sheet in crushing, bending, pile-up and ride-up modes have been estimated. Force associated with buckling failure will now be investigated where an ice sheet is loaded over a limited contact area.

In the past, investigators have considered the buckling of a floating ice sheet using the buckling analysis of a beam on an elastic foundation. The inherent assumption in the use of this analysis requires that the forces act uniformly on the edge of the ice sheet. The resulting high force levels required to cause failure led the investigators to conclude that the available driving forces were only sufficient to allow thin ice sheets to fail in the buckling mode (Assur 1971, Kry 1980). However, recent buckling analyses of a floating ice sheet by Sodhi and Hamza (1977), Wang (1978a, b) and Sodhi (1979) allow for the consideration of the buckling failure of a large ice sheet when it is in contact with a wide structure or a beach over a limited area.

To investigate all possible situations for buckling failure, an idealized wedge-shaped ice sheet is considered, as depicted in Figure 47. The ice sheet is shown to be loaded by a total force F acting along the curved leading edge, such that it creates

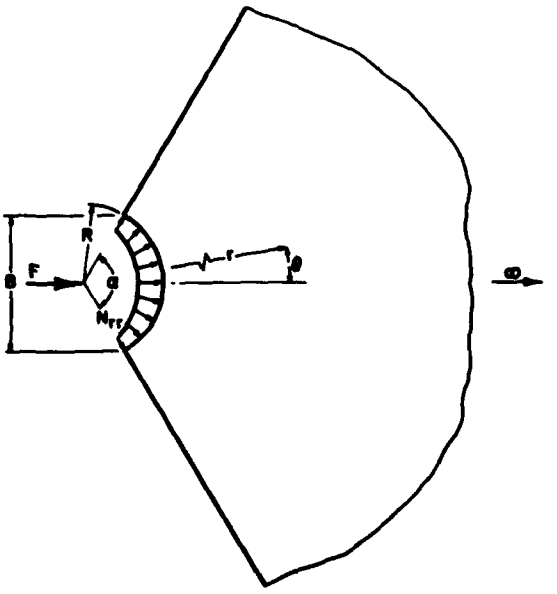

Figure 47. Geometry of a wedge-shaped floating ice sheet. Note that the arrows show the stress distribution along the area of contact change with the cosine of θ and these sum up to a total force F.

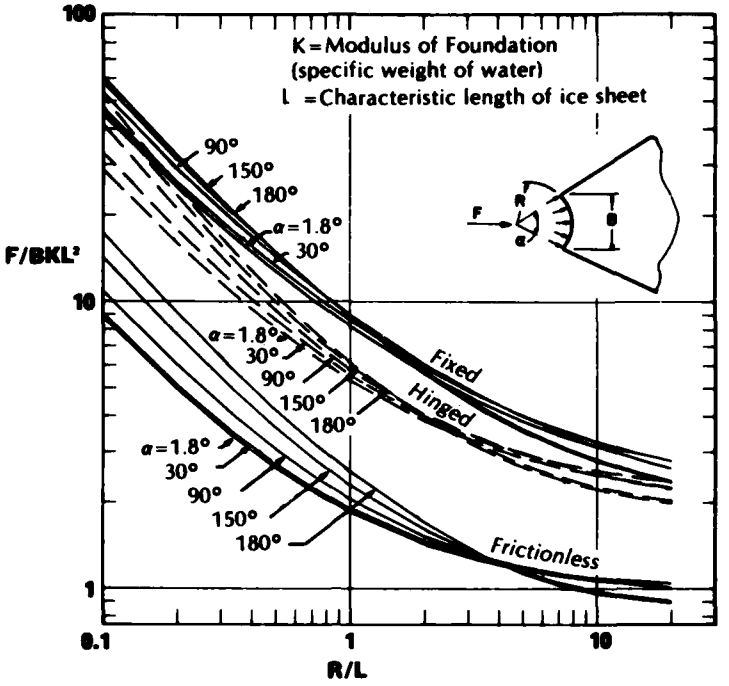

Figure 48. Non-dimensional buckling load for different ice sheet wedge angles α, R/L values and buckling conditions (from Sodhi 1979).

a radial (compressive,-) stress field $N_{rr} = -[2F/(\alpha+\sin\alpha)][\cos\theta/r]$ N/m in the ice sheet. The symbols used in this equation are graphically explained in Figure 47. The non-dimensional buckling loads for wedge-shaped floating ice sheets have been given by Sodhi (1979), and these are presented graphically in Figure 48 for different wedge angles, R/L values and boundary conditions. We may write the non-dimensional buckling load as follows:

$$\frac{F}{BKL^2} = f\left(\frac{R}{L}, \alpha, \text{boundary condition}\right) \quad (8)$$

where K = foundation modulus (equal to the specific weight of water in the case of floating ice)
$L = [Eh^3/[12(1-\nu^2)K]]^{1/4}$, characteristic length of ice sheet
ν = Poisson's ratio
E = ice sheet modulus of elasticity
h = ice sheet thickness
$B = 2R\sin(\alpha/2)$ (width of contact area).

Since the non-dimensional buckling load is not influenced strongly by the wedge angle α (Fig. 48), our discussion is restricted to a particular value of $\alpha = 180°$ (i.e. semi-infinite ice sheet). During the course of recent experiments (Sodhi et al. 1982) it was observed that the non-dimensional buckling loads from theory (Sodhi 1979) and experiments are in close agreement. It was also observed that the boundary condition at the ice/structure interface corresponds to a situation between the frictionless and hinged boundary conditions. Unless ice freezes to the structure, the fixed boundary condition is not likely to occur. Hence the buckling loads corresponding to the hinged and the frictionless boundary conditions are the upper and lower bounds. The expression for the pressure at the contact area required to buckle an ice sheet is:

$$p_b = (F/Bh)$$

$$= KL(L/h)f(R/L, \alpha, \text{boundary condition}) \quad (9)$$

Assuming values of $E = 10^9$ Pa (0.145×10^6 psi), $K = \rho_w g = 10.1$ kN/m³ (64.3 lb/ft³) and $\nu = 0.33$, we calculated the buckling pressures shown in Table 3 for different values of R/L, and ice thicknesses for the frictionless and hinged boundary conditions. From these buckling pressure values it can be seen that, for a particular ice thickness, if the area of contact is small, a large pres-

Table 3. Buckling pressure for different R/L and boundary conditions.

				R/L					
				0.1		1.0		10	
h		L		Buckling pressure					
(m)	(inch)	(m)	(ft)	(MPa)	(psi)	(MPa)	(psi)	(MPa)	(psi)
Frictionless Boundary Condition									
0.3	(11.8)	3.98	(13)	9.23	(1339)	1.36	(198)	0.51	(74)
0.5	(19.7)	5.83	(19)	11.92	(1729)	1.76	(255)	0.66	(96)
1.0	(39.4)	9.81	(32)	16.86	(2445)	2.49	(361)	0.93	(135)
1.5	(59.1)	13.30	(44)	20.65	(2995)	3.05	(442)	1.14	(166)
Hinged Boundary Condition									
0.3	(11.8)	3.98	(13)	27.54	(3995)	3.26	(473)	1.18	(171)
0.5	(19.7)	5.83	(19)	35.55	(5157)	4.21	(610)	1.52	(221)
1.0	(39.4)	9.81	(32)	50.28	(7293)	5.95	(863)	2.15	(313)
1.5	(59.1)	13.30	(44)	6.158	(8932)	7.28	(1057)	2.64	(383)

sure is required to initiate ice sheet buckling, whereas the buckling pressure is relatively low when the area of contact is large.

However, if the contact area is small, high stress can be created along the boundary by a relatively low far-field stress in the ice sheet. This is due to the fact that the radial stress decreases as the inverse of the radial distance from the wedge apex. In fact it is possible that the ice sheet will fail in the *crushing mode rather than in the buckling mode if* the effective crushing pressure is less than the buckling pressure for small contact area. This was shown to be the case where ice was shown failing against a man-made gravel island in a movie presented by D. McGonigal of Gulf Canada Resources, Inc. at the October 1980 National Research Council Workshop on Sea Ice Ridging held in Calgary, Alberta. As the ice is crushed, the contact area becomes enlarged and the effective modulus of elasticity of the ice sheet becomes lower due to cracking activity. Both of these effects lower the pressure required to buckle the ice sheet. If the ice sheet buckles, it produces jagged ice edges which in turn promote more crushing and buckling at other locations as the ice sheet moves towards a wide object, be it a structure, beach or rubble pile. Again, this was apparent in the McGonigal film mentioned above. The phenomenon of a "complex combination of continuous crushing and buckling" was also reported for the ice failing around Netserk F40, an artificial "gravel" island (Gladwell 1977).

If the contact areas are regularly spaced at a distance of λ times the characteristic length, then the far-field ice pressure (σ_{ff}) required to buckle the ice sheet at all the contact areas simultaneously is:

$$\sigma_{ff} = (2R/L)\sin(\alpha/2)\,p_b/\lambda \qquad (10)$$

where p_b is given by eq 7.

To illustrate the usefulness of the above equation, we consider a semi-infinite ice sheet (i.e. $\alpha = 180°$) and we take $R/L = 1.0$ because smaller contact areas would likely cause crushing and large contact areas are less likely to occur. Based on these assumptions the far-field ice pressures needed to cause buckling of a semi-infinite ice sheet are listed in Table 4.

In a short version of this report presented at POAC-81 (Kovacs and Sodhi 1981), P.R. Kry brought up the point that the spacing λ of the locations where buckling occurs is given as an independent parameter in Table 4:

> "The mean stress presented in the table thus decreases significantly as λ increases because it assumes there is more area over which the driving stress is applied (λL); whereas the failure load is a constant being restricted to single areas separated by increasing distance.
>
> "This is questionable on the grounds that the spacing λ is, in general, determined by the failure process. For buckling failures the cusps, giving rise to individual subsequent failures, will have a spacing of only a few action radii ($\lambda << 10$). λ values higher than this may not be physically reasonable."

We agree that the spacing of contact areas is determined by the size of cusps or the area of the ice sheet affected by buckling failure. The spacing parameter was arbitrarily assumed to demonstrate that low environmental forces can cause buckling failure in an ice sheet. It should also be pointed out that the above situation refers to the case when all buckling failures occur simultaneously. If non-

Table 4. Far-field ice pressure required to buckle a semi-infinite ice sheet when the contact areas are spaced λ times the characteristic length. Each contact area is twice as wide as the characteristic length.

				λ							
				5		10		20		50	
h		*L*		*Far-field ice pressure*							
(m)	*(in.)*	*(m)*	*(ft)*	*(MPa)*	*(psi)*	*(MPa)*	*(psi)*	*(MPa)*	*(psi)*	*(MPa)*	*(psi)*
Frictionless Boundary Condition											
0.3	(11.8)	3.98	(13)	0.55	(79)	0.27	(40)	0.14	(20)	0.05	(8)
0.5	(19.7)	5.83	(19)	0.70	(102)	0.35	(51)	0.18	(26)	0.07	(10)
1.0	(39.4)	9.81	(32)	1.00	(144)	0.50	(72)	0.25	(36)	0.10	(14)
1.5	(59.1)	13.30	(44)	1.22	(177)	0.61	(88)	0.30	(44)	0.12	(18)
Hinged Boundary Condition											
0.3	(11.8)	3.98	(13)	1.30	(189)	0.65	(95)	0.33	(47)	0.13	(19)
0.5	(19.7)	5.83	(19)	1.68	(244)	0.84	(122)	0.42	(61)	0.17	(24)
1.0	(39.4)	9.81	(32)	2.38	(345)	1.19	(173)	0.59	(86)	0.24	(35)
1.5	(59.1)	13.30	(44)	2.91	(423)	1.46	(211)	0.73	(106)	0.29	(42)

simultaneous failure zones are assumed to occur, the values given in Table 4 may not be so unreasonable.

From the above reasoning it is evident that the ice sheet may fail in either crushing or buckling, if the ice contact areas are either very small or are spaced at distances in excess of ten times the characteristic length.

DRIVING FORCES

In addition to considering the forces associated with the different types of ice failure modes against the rock, it is appropriate to also consider the environmental driving forces. Ice forces on the rock will be governed by the ice thickness, failure mode, and available driving forces.

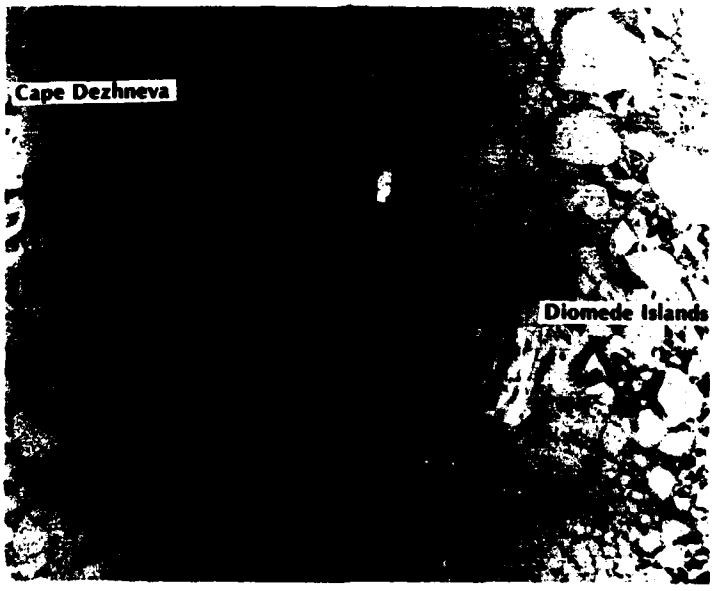

Figure 49. Ice floes in the Bering Strait. For reference Big Diomede Island is about 10 km long.

The dominant factors affecting ice motion and forces in the Bering Strait are wind and water drag on the ice cover. Internal ice stresses are small because of the open nature of the pack. Consider a large (10-km-square) floe impinged against the north side of Fairway Rock acted upon by southward 30-m/s winds and 1.5-m/s currents. Using the drag coefficients given by Pritchard et al. (1979) for ice in the Bering Strait, we can calculate the ice driving forces on the rock from

$$F = (\varrho_a c_a V_a^2 + \varrho_w c_w V_w^2) L^2 \qquad (11)$$

where ϱ_a = air density
c_a = ice–air drag coefficient
V_a = air velocity
ϱ_w = water density
c_w = ice–water drag coefficient
V_w = water velocity
L = floe size.

For $\varrho_a c_a = 1.1 \times 10^{-3}$ kg/m³ and $\varrho_w c_w = 8$ kg/m³ and the assumed winds and currents, a driving force of 1900 MN (4.27×10^8 lb) is obtained. If both the winds and currents were reduced by a factor of 2, we would still obtain a driving force of 475 MN (1.07×10^8 lb). As 10-km-square floes are not uncommon (Fig. 49), these calculations suggest that all five of the ice failure modes considered are feasible in the vicinity of Fairway Rock.

ANGLE OF INTERNAL FRICTION OF SEA ICE

As the ice moves past an island in deep water it fails, forming a wedge-shaped rubble formation. If we assume that the ice floes represent a material which can be characterized by a Mohr-Coulomb type failure criterion, we can estimate its angle of internal friction. The angle between the wedge side (shear boundary) and the wedge base represents the angle between the intermediate plane and the plane of major principal stress. Knowing this angle, the angle of internal friction ϕ at the shear boundary can be determined from $\theta = 45° - \phi/2$. However, determination of ϕ is not always easy because both island geometry and differential erosion of the ice rubble can distort the wedge shape, making it difficult to locate the position of the wedge base. This can be resolved by assuming that the base apex angles of the wedge are the same. It then follows that θ is equal to $(180° - \alpha)/2$, where α is the angle formed at the intersection of the wedge sides (Fig. 50). Since α is equal to $90° - \phi$, it is then possible to determine ϕ by knowing α. This

Figure 50. Ice wedge developed on the south side of the Diomede Islands, 2 April 1975. The angle of internal friction, ϕ, is equal to $90° - \alpha$.

Figure 51. Ice wedge developed on the south side of the Diomede Islands, 11 April 1975.

methodology was used by Kovacs (1976) in a study of snow displaced along piles driven into snow and Sodhi (1977) in the analysis of a wedge-shaped ice formation north of St. Lawrence Island.

The apparent angle α was measured for five wedge-shaped formations at Fairway Rock, five formations that formed on either the north or the south side of the Diomede Islands (Fig. 51), and two formations that formed on the north side of St. Lawrence Island. These angles varied from 50° to 70° and averaged 60°. From this average the angle of internal friction was determined to be 30°. This angle may be compared to the results of other investigations: model shear box values found by Keinonen and Nyman (1978) of 47°, Prodanovic (1979) of 47° and 53°, and Weiss et al. (1981) of 11° to 34° with an average of 22°; the average angle of repose of ice blocks in first-year pressure ridge sails found by Kovacs (1972) of 24°, Gladwell (1976) of 34°, and Tucker and Govoni (1981) of 26°; the average angle of repose of ice blocks in shore ice pile-ups found by Kovacs et al. (1975) of 32° and Kovacs (1982) which varied from 30 to 45° and averaged 37°; the average value of 33° found in this study for the ice blocks in the ridges at Fairway Rock; the average angle of repose of ice blocks in first-year pressure ridge keels found by Kovacs (1972) of 33°; and the values obtained from triaxial tests on first-year sea ice by Panov and Fokeev (1977), which varied from 14° to 55°.

Differences in test conditions, ice stress state, and ice properties may be invoked to explain much of the large variation in the above ϕ values. Ice stress state and ice properties were clearly shown by Panov and Fokeev (1977) to affect ϕ. However, the lower slope angles of Kovacs (1972) and Tucker and Govoni (1981) are the result of these investigators' desire to characterize the relative shape of the ridge sail. They were not specifically interested in the angle of repose of the ice blocks. Higher values, which average 29°, result when the slope of the ice blocks is measured near the peak of the ridges, as studied by Kovacs (1972). In this way the effect of nonuniform ice piling, which can cause highly irregular ridge slopes, is minimized. For purposes of determining the angle of ice block friction, the latter measurement is preferred, provided a "sufficient" number of ice blocks exist in the ridge face to establish a representative angle of repose.

From the above determinations and observations, a representative value for the angle of internal friction of sea ice would appear to be between 30° and 35°.

SUMMARY

The information obtained in this study revealed that Fairway Rock was surrounded by a massive icefoot in the winter of 1980. This icefoot was the result of ice impacting the island, failing, and subsequently piling up, forming ridges up to 15 m high. The icefoot varied from less than 10 to over 100 m wide. The slope of the inner ridges averaged 33° while the slope of the outer face of the icefoot was in excess of 70°. This was apparently the result of nongrounded ice rubble having slumped or been cleaved off. The instructive findings are, as anticipated, that ice rubble formation around a large structure placed in "deep" water will not extend appreciably beyond the width of the structure, and therefore will not add significantly to its effective diameter. In order for this to be so, the submarine slope needs to be relatively steep. At Fairway Rock, it is reasonable to assume that the shallowest submarine slope was at or near the angle of repose of the rock talus.

Fairway Rock and Little Diomede Island were observed encrusted with a thick icing layer that extended high above sea level. For offshore structures placed in these waters, this phenomenon needs to be considered from a loading as well as an operational hindrance standpoint. For detailed information on the subject of icing formation in general, and ocean structure icing in particular, see Minsk (1977, 1980) and Stallabrass (1980).

Shear ridge rubble fields observed in this study near Prince of Wales Shoal were found to reach heights on the order of 6 m, with an apparent average of 2 m. The average ice thickness was estimated to be 11 m. These rubble fields are, on occasion, driven south, and therefore represent one of the major ice features to be considered in the design of a structure placed in these waters.

The ice force levels given here are *only estimates* based upon assumed ice data and geometry considerations. Larger forces are possible at local contact points where stress is concentrated. The calculated effective pressures due to creep, crushing and flexural failure of ice 1.5 m thick against Fairway Rock were estimated to be 1630 kPa (236 psi), 1930 kPa (280 psi), and 394 kPa (57 psi), respectively. An analysis of the available driving forces suggests that all three failure modes are possible. However, out of the three possible modes of failure, the ice cover would most likely fail in flexure, as opposed to crushing, since it requires less force.

We have also presented expressions to show that buckling is also entirely possible at areas of local sheet ice contact, even when the far-field ice pres-

sure is relatively low. Indeed, we envision that all three failure modes will occur randomly during ice failure against a large structure or during ice pack deformation.

Finally, examination of ice wedges against various islands in the Bering Sea suggests that the angle of internal friction of sea ice is about 30°.

LITERATURE CITED

Ahlnas, K. and G. Wendler (1979) Sea-ice observations by satellite in the Bering, Chukchi and Beaufort Seas. In *Proceedings, Fifth International Conference on Port and Ocean Engineering Under Arctic Conditions,* Norwegian Institute of Technology, Trondheim, Norway.

Assur, A. (1971) Forces in moving ice fields. In *First International Conference on Port and Ocean Engineering Under Arctic Conditions,* Trondheim, Norway, vol. I.

Bloom, G.L. and D.E. McDougal (1967) Bering Strait unattended oceanographic telemetry system utilizing a commercial LCC-25 strontium 90 generator. *The New Thrust Seaward.* Transactions of the Third Annual Marine Technological Society Conference and Exhibit, 5-7 June, San Diego, California. Washington, D.C.: Marine Technological Society.

Coachman, L.K. and K. Aagaard (1966) On the water exchange through Bering Strait. *Limnological Oceanography,* vol. 1, no. 1.

Coachman, L.K. and K. Aagaard (1979) Re-evaluation of water transports in the vicinity of Bering Strait. Preprint of paper to appear in *The Bering Sea Shelf: Oceanography and Resources* (W.D. Hood and J.A. Calder, Eds.). Juneau, Alaska: U.S. Dept. of Commerce, NOAA Alaska Office of Marine Pollution Assessment.

Croasdale, K.R. (1980) Ice forces on fixed, rigid structures. In *Working Group on Ice Forces on Structures: A State-of-the-Art Report* (T. Carstens, Ed.). U.S. Army Cold Regions Research and Engineering Laboratory, CRREL Special Report 80-26. ADA-089674.

Gladwell, R.W. (1976) Field studies of eight first-year sea-ice pressure ridges in the southern Beaufort Sea. Imperial Oil Limited, Production Research Division Report IPRT-8ME-76, APOA Project No. 75, Calgary, Alberta, Canada.

Gladwell, R.W. (1977) Ice conditions around artificial islands 1975 to 1976. ESSO Resources Canada Ltd., Production Research Division, Calgary, Alberta, Canada, Arctic Petroleum Operators Association Report No. 105-3.

Keinonen, A. and T. Nyman (1978) An experimental model-scale study of the compressibility, friction and cohesive behavior of broken ice mass. IAHR Symposium on Ice Problems, Lulea, Sweden.

Kovacs, A. (1972) On pressured sea ice. In *Proceedings, International Conference on Sea Ice* (T. Karlason, Ed.). Reykjavik, Iceland: National Research Council.

Kovacs, A. (1976) Study of piles installed in polar snow. CRREL Report 76-23. ADA-029191.

Kovacs, A. (1982) Recent shore ice ride-up and pile-up observations. Part I: Beaufort Sea, Alaska. (In press.)

Kovacs, A. and M. Mellor (1974) Sea ice morphology and ice as a geologic agent in the southern Beaufort Sea. In *The Coast and Shelf of the Beaufort Sea* (J.C. Reed and J.E. Sater, Eds.). Arlington, Va.: Arctic Institute of North America.

Kovacs, A., D. Dickens and B. Wright (1975) Multi-year pressure ridge and shore ice pile-up. Arctic Petroleum Operators Association Project 89.

Kovacs, A. and D.S. Sodhi (1980) Shore ice pile-up and ride-up: Field observations, models, theoretical analyses. *Cold Regions Science and Technology,* vol. 2.

Kovacs, A. and D.S. Sodhi (1981) Sea ice piling at Fairway Rock, Bering Strait, Alaska: Observations and theoretical analyses. *Proceedings, Sixth International Conference on Port and Ocean Engineering Under Arctic Conditions,* University of Laval, Quebec, Canada, vol. II and III.

Kry, P.R. (1977) Ice rubble fields in the vicinity of artificial islands. *Proceedings, Fourth International Conference on Port and Ocean Engineering Under Arctic Conditions,* Memorial University of Newfoundland, St. John's, Newfoundland, Canada.

Kry, P.R. (1978) A statistical prediction of effective ice crushing stress on wide structures. *Proceedings, International Association of Hydraulic Research Symposium on Ice Problems,* Lulea, Sweden.

Kry, P.R. (1980) Ice forces on wide structures. *Canadian Geotechnical Journal,* vol. 17.

Michel, B. (1970) Ice pressure on engineering structures. CRREL Monograph III-B1b. AD-709625.

Michel, B. and N. Toussaint (1976) Mechanism and theory of indentation of ice plates. Symposium on Applied Glaciology, Cambridge, England. *Journal of Glaciology,* vol. 19, no. 81.

Minsk, L.D. (1977) Ice accumulation on ocean structures. CRREL Report 77-17. ADA-044258.

Minsk, L.D. (1980) Icing on structures. CRREL Report 80-31. ADA-095474.

More, D.G. (1964) Acoustic-reflection reconnaissance of continental shelves: Eastern Bering and Chukchi Seas. *Papers in Marine Geology,* Shepard Commemorative Volume (R.L. Miller, Ed.). New York: Macmillan.

Muench, R.D. and K. Ahlnas (1976) Ice movement and distribution in the Bering Sea from March to June 1974. *Journal of Geophysical Research,* vol. 81.

Panov, V.V. and N.V. Fokeev (1977) Compression strength of sea ice specimens under complex loading. *Problemy Arktiki i Antarktiki,* vol. 49.

Porter, A.R.S., A.C. Palmer, D.J. Doogman, M.F. Ashby, A.G. Evans and J.W. Hutchinson (1981) The force exerted by a moving ice sheet on an offshore structure. I: The creep mode. Unpublished manuscript, Center for Cold Ocean Resources, Memorial University of Newfoundland, St. Johns, Newfoundland.

Parmerter, R.R. and T.D. Coon (1973) Model of pressure ridge formation in sea ice. *Journal of Geophysical Research,* vol. 77, no. 33.

Pritchard, R.S., R.W. Reimer and M.D. Coon (1979) Ice flow through straits. *Proceedings, Fifth International Conference on Port and Ocean Engineering Under Arctic Conditions,* Norwegian Institute of Technology, Trondheim, Norway.

Prodanovic, A. (1979) Model tests of ice rubble strength. *Proceedings, Fifth International Conference on Port and Ocean Engineering Under Arctic Conditions,* Norwegian Institute of Technology, Trondheim, Norway.

Ralston, T.D. (1979) Sea ice loads. Presented at Technical Seminar on Alaskan Beaufort Sea Gravel Island Design, Exxon Company, Houston, Texas.

Reimer, R.W. (1979) Ice breakout in the Bering Strait. Master of Engineering thesis, University of Washington, Seattle, Washington.

Selkregg, L.L. (1976) Alaska regional profiles, Yukon region. Vol. VI. Arctic Environmental Information and Data Center, University of Alaska.

Shapiro, L. and J.J. Burns (1975) Satellite observations of sea ice movement in the Bering Strait regions. In *Climate of the Arctic* (G. Weller and S.A. Bowling, Eds.). Proceedings of the

AAAS–AMA Symposium, Fairbanks, Alaska, August 1973. Geophysical Institute, University of Alaska.

Shumway, G., D.G. More and G.B. Dowling (1964) Fairway Rock in Bering Strait. *Papers in Marine Geology*, Shepard Commemorative Volume (R.L. Miller, Ed.). New York: Macmillan.

Sodhi, D.S. (1977) Ice arching and the drift of pack ice through restricted channels. CRREL Report 77-18. ADA-044218.

Sodhi, D.S. (1979) Buckling analysis of a wedge-shaped floating ice sheet. *Fifth International Conference on Port and Ocean Engineering Under Arctic Conditions*, Norwegian Institute of Technology, Trondheim, Norway.

Sodhi, D.S. and H.E. Hamza (1977) Buckling analysis of a semi-infinite ice sheet. *Fourth International Conference on Port and Ocean Engineering Under Arctic Conditions*, Memorial University ofNewfoundland, St. John's, Newfoundland.

Sodhi, D.S., F.D. Haynes, K. Kato and K. Hirayama (1982) Experimental determination of the buckling loads of floating ice sheets. 2nd International Symposium on Applied Glaciology, CRREL, Hanover, N.H., 23–27 August 1982.

Stallabrass, J.R. (1980) Trawler icing: A compilation of work done at N.R.C. National Research Council of Canada Report NRC-19372.

Stringer, W.J. (1978) Morphology of Beaufort, Chukchi and Bering Sea nearshore ice conditions by means of satellite and aerial remote sensing. Geophysical Institute Report, University of Alaska, Fairbanks, Alaska.

Tucker, W.B., III and J.W. Govoni (1981) Morphological investigations of first-year sea-ice pressure ridge sails. *Cold Regions Science and Technology*, vol. 5, no. 1.

Wang, Y.S. (1978a) Buckling analysis of a semi-infinite ice sheet moving against cylindrical structures. *Proceedings, International Association of Hydraulic Research Symposium on Ice Problems*, Lulea, Sweden.

Wang, Y.S. (1978b) Buckling of a halt ice sheet against a cylinder. *Proceedings, ASCE, Journal of Engineering Mechanics Division*, EM5.

Wang, Y.S. (1979) Sea ice properties. Presented at Technical Seminar on Alaskan Beaufort Sea Gravel Island Design, Exxon Company, Houston, Texas.

Weiss, R.T., A. Prodanovic and K.N. Wood (1981) Determination of ice rubble shear properties. IAHR International Symposium on Ice, Quebec City, Quebec, Canada.

APPENDIX A: APRIL 1982 FIELD OBSERVATIONS AT FAIRWAY ROCK

During the first week of April 1982, a short visit to Fairway Rock was made. There was a strong breeze coming out of the south. This driving force, coupled with that of the northward current flow, was pushing 1-m-thick sea ice past the rock at about 1 km/hr. The icefoot was again noted to be composed of densely packed sea ice rubble up to 15 m high, and the rock walls were observed in places to be covered with a thick glazing of ice to an elevation of over 30 m (Fig. A1).

Ice floes were seen being driven against the icefoot (Fig. A2), and were undergoing failure in the following ways:

A. An ice floe would contact the icefoot and begin to crush or fail in flexure along the contact areas. This would be followed by splitting of the floe into two or more fragments, followed by renewed crushing or flexural failure at the icefoot contact areas.

B. A floe would contact the icefoot, stop, and undergo crushing or flexural failure upstream of the contact area. During this process, ice ridging would occur. These ridges were typically less than 2 m high.

C. A floe would contact the icefoot, undergo crushing or flexural failure at the impact areas,

Figure A1. View of Fairway Rock icefoot and glaze ice formation. Top photo shows southeast side of rock; bottom photo shows northeast side.

and then split. A portion of the floe would then be driven past the rock, where it would undergo continuous crushing and flexural failure as it moved along the icefoot shear boundary. During this process much of the broken ice was reduced to rubble with dimensions less than the thickness of the ice floes.

D. An ice floe would contact the icefoot and undergo complete disaggregation by crushing and flexural failure.

We noted that crushing of ice floes at the base of the icefoot was a common mode of failure and during our observations appeared to occur over half the width of the icefoot. During crushing, the resulting ice blocks were typically less than half the thickness of the ice in the floe being crushed. Standing near the failure zone, we noted that the ice sheet did not appear to be moving up or down during crushing.

During our visit the icefoot was not "growing." The ice which had failed and piled up against the icefoot would from time to time appear to cave in or slump downward. The ice keel of the rubble was apparently undermined by the strong current, which transported the submerged ice blocks away.

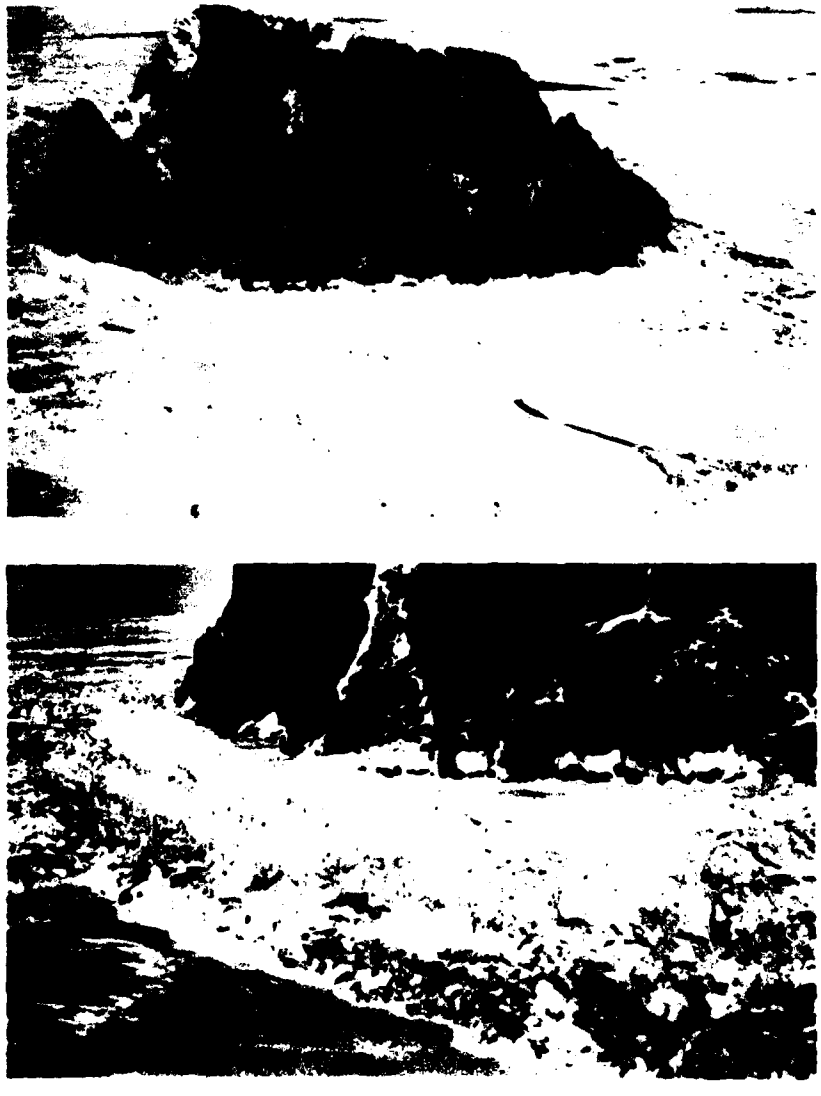

Figure A2. Ice floes against the southern Fairway Rock icefoot. The discolored ice blocks are contaminated with biological organisms. These blocks resulted from crushing of the parent floe.

A facsimile catalog card in Library of Congress MARC format is reproduced below.

Kovacs, A.
Bering Strait sea ice and the Fairway Rock icefoot, by A. Kovacs, D.S. Sodhi and G.F.N. Cox. Hanover, N.H.: U.S. Cold Regions Research and Engineering Laboratory; Springfield, Va.: available from National Technical Information Service, 1982.
iv, 44 p., illus.; 28 cm. (CRREL Report 82-31.)
Bibliography: p. 37.
1. Ice. 2. Sea ice. 3. Ice forces. I. Sodhi, D.S. II. Cox, G.F.N. III. United States. Army. Corps of Engineers. IV. Army Cold Regions Research and Engineering Laboratory, Hanover, N.H. V. Series: CRREL Report 82-31.

☆U.S. GOVERNMENT PRINTING OFFICE: 1982 – A-2294/258